IIASA's Work on Climate Change: Assessing Environmental Impacts

M. Jonas, K. Olendrzyński, J. Krabec, and R. Shaw

Contents

Foreword

This Status Report is adapted from a lecture presented by Matthias Jonas at the Institute for Meteorology and Geophysics, University of Vienna, May 1992. In his lecture, Dr. Jonas clearly summarizes the status of the work being carried out within the Climate Change Projections Study at IIASA. This work involves linking a policy-oriented climate change model, the Integrated Model to Assess the Greenhouse Effect (IMAGE), to models of ecological change such as the Global Vegetation Model, the Timber Assessment Model, and the Regional Acidification INformation and Simulation (RAINS) model. These models were at least partially developed at IIASA. The result of this linkage work, which is being carried out in collaboration with the Netherlands National Institute of Public Health and Environmental Protection (RIVM), and possibly other institutes, is intended to be a tool to help policy makers assess in a rapid and time-dependent way changes in regional ecology resulting from various greenhouse gas emission scenarios.

Roderick Shaw
Leader
Climate Change Projections Study

IIASA's Work on Climate Change: Assessing Environmental Impacts

1. Introduction

The Climate Change Projections Group is part of the Environmental Change and Development Project headed by Dr. Rod Shaw. The aim of the climate modeling group is to link their work with environmental impact models in an integrated and time-dependent fashion. In this report three environmental impact models are described. The climate models which were studied before switching over to a *two-dimensional Energy Balance Model (2-D EBM)* are also described. We think the 2-D EBM will cope with the computational needs of the environmental impact models we are studying.

2. Environmental Impact Models

Until about three decades ago, the idea that the environment is not an inexhaustible resource was not generally accepted; at that time only local air and water pollution was given any serious attention. Since then, however, it has become clear that a number of other severe threats to the environment require urgent attention and internationally coordinated actions. These threats include (from Döös, 1991, modified):

- The acidification of terrestrial and aquatic ecosystems caused mainly by the increasing emission of sulfur dioxide (late 1960s).
- The threats to the tropical forests mainly caused by socioeconomic factors, and the irreversible loss of biodiversity (late 1960s).

1

- The climatic change caused by the increasing atmospheric concentration of carbon dioxides (early 1970s).
- The destruction of the stratospheric ozone layer caused mainly by the use of chlorofluorocarbons (mid-1970s).
- Recognition of the fact that several greenhouse gases in addition to carbon dioxide contribute substantially to the change of climate (early 1980s).

The very fact that new major environmental problems have unexpectedly appeared within the interval of a few years does not provide any confidence that we now are aware of all the possible threats.

Models are available for many environmental impacts falling under these and related topics. Usually these models are self-standing; they are not part of an *integrated system* or *assessment model* which starts, say in the case of climate change, with a greenhouse gas energy-emission accounting framework for the simulation of anthropogenic activities and ends with the environmental impact itself. *Figure 1* gives an overview of some selected environmental impacts for which assessment models are ready to be linked to an *integrated climate model*.

What kind of information do we try to gain from a linkage? Of course, the answer depends on the respective combination of the impact model and the integrated climate model. Some of these models are described below.

2.1 Timber Assessment Model

IIASA's Timber Assessment Model (TAM) of the Forestry Resources Project addresses the economic, ecological, and social consequences of the future development of forest resources. The immediate focus is on the effects of air pollution and climate change.

TAM consists of two parts (Nilsson *et al.*, 1991, 1992): a detailed country-by-country database on forest resources in Europe and a simulation model, or more precisely a matrix-type simulation model. The structure of TAM is illustrated in *Figure 2*.

The parameters of the database specify the forest state, i.e., species composition, age classes, standing volume, owner categories, and external alterations to the initial conditions such as changes in the forest landbase. This allows one to establish an age-volume matrix for each forest type (*Figure 3*). Here, the concept of forest is used for a stratum that can be defined by country, geography, owner, forest structure (high forest, coppice), site class,

POLICY OPTIONS

2-D Energy Balance Model (EBM)
to be linked with RIVM's
Integrated Model to Assess the Greenhouse Effect
(IMAGE)

1 2 3 4 5

IIASA
Timber Assessment
Model

IIASA ?
H(C)FC Impact on
National Health
Systems

RIVM, IIASA
Global Vegetation
Model (GVM)

RIVM
Sea Level Rise

IIASA, IBM/N, EMEP
Long Range Transport of Air
Pollutants (LRTAP) Models
and
Regional Acidification INformation
and Simulation (RAINS) Model

Figure 1. Envisaged dynamical linkages with environmental impact models.

4

Database

- Parameters describing the forest state

  species composition, age classes, standing volume,
  external alterations to initial conditions, ...

- Parameters describing biological dynamics

  growth, mortality, seed production and disposal,
  site quality, ...

- Parameters describing human management activities
  and external factors influencing the dynamics

  plantation and thinning intensity, rotation periods, species
  selection, ...; air pollutants, ...

Matrix-type simulation model

The TAM deals with

- representation of forest growth
- reactions to changes in the environment
- reactions to changes in management programs
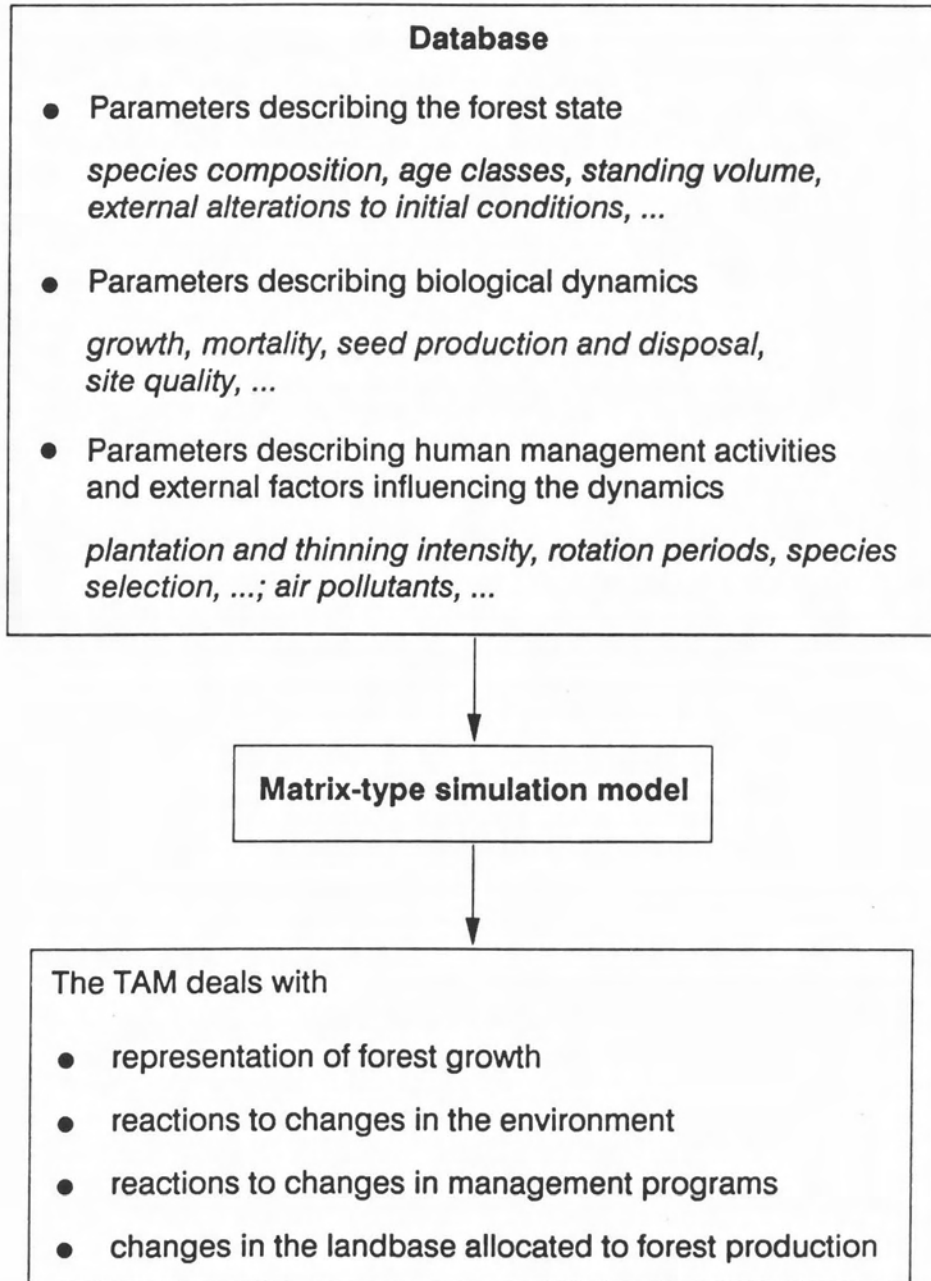- changes in the landbase allocated to forest production

Figure 2. Structure of the Timber Assessment Model (TAM). Sources:
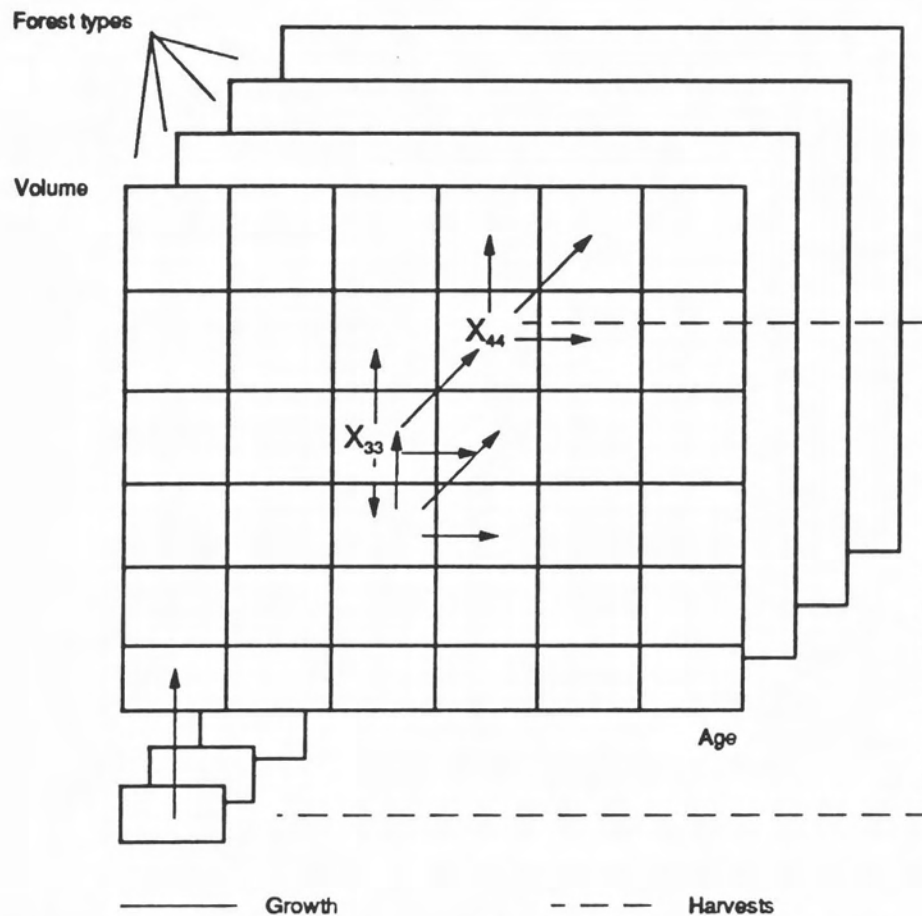Nilsson *et al.*, 1991, 1992.

Figure 3. Transitions in the area model. Source: Nilsson *et al.*, 1992.

and species. The volume dimension of the matrix is defined by about 10 intervals and the age dimension by 6 to 15 intervals. The forest state is then depicted by an area distribution over this matrix.

Two other parameter sets are needed to make the matrix dependent on time and thus have a dynamical behavior. These are parameters describing biological dynamics (growth, mortality, regeneration); and parameters influencing human management activities (plantation and thinning intensities, rotation periods, species selection) and external factors (air pollutants).

Dynamics in terms of volume increments are expressed as transition of areas between specific fixed states in the matrix. Thus the existing TAM can

deal with the representation of forest growth, responses to different forest management and forest policies, reactions to changes in the environment such as forest decline attributed to air pollutants, and responses to changes in the landbase allocated to forest production.

An assumed change in climate will influence the so-called species life history parameters, such as maximum and minimum annual effective temperature sum, shade and drought tolerance, and seed crop production, and thus the parameters describing the biological dynamics. Climate change will also influence parameters dealing with the current silviculture management programs. Given the many uncertainties in the change of biological parameters, the changes in surface temperature and precipitation resolved for 10° latitude belts are considered to be the key climate quantities to be handed over from the climate model to TAM. Moreover, the use of more detailed climatic information on spatial resolution is questionable in view of the uncertainties associated with climate predictions in both time and space (IPCC, 1990).

It is difficult to predict the results of linking TAM to an integrated climate model. So far we have only limited knowledge about possible negative and positive effects on the behavior of forest ecosystems, especially in mountain areas. In addition to the possible direct fertilization effect of CO_2 and the effect of temperature and precipitation changes, a number of other factors might strongly influence the rate and extent of forest reactions. These factors include the availability of nutrients and soil water; the increased activities of and vulnerability to microbial pathogens, insects, and diseases; and forest fires. Nilsson and Pitt (1991) give some estimates of the climatic effects on forest production and silviculture for various regions in Europe (*Table 1*). However, it is important to point out that these estimates are based mainly on knowledge from managed industrial forests, whereas most European mountain forests are not industrial forests but protected forests and parks with very specific management systems.

2.2 Global Vegetation Model

The second model which has a great potential for agricultural, biogeographical, and ecological studies is IIASA's *Global Vegetation Model (GVM)*; this model also includes forests. The Biosphere Dynamics Project developed a climate database which is entirely based on climate records, and embodied it within a *Geographical Information System (GIS)*. This permits instant visualization of current climatic conditions and their effect on life and vegetation-

Table 1. Forest production and silvicultural management responses to climate change in selected areas and countries.

Region	Forest production	Silvicultural implications
Nordic countries	Increased production	Intensified management of all phases of silviculture
Northern USSR	Increased production	Intensified management of all phases of silviculture
Middle-belt USSR	Increased production in the western part	Intensified management in the western part
Southern USSR	Decreased production	Intensified protection forest management; intensified sanitation and fire protection
Denmark Benelux France United Kingdom Ireland	Increased production	Intensified management of all phases of silviculture
Germany Poland CSFR Lower Austria Switzerland	Increased production	Intensified management of all phases of silviculture
Mountainous areas: France Germany Austria Switzerland Italy	Decreased production	Intensified protection forest management; intensified sanitation and fire protection
Hungary Bulgaria Romania Yugoslavia Albania	Decreased production	Intensified protection forest management; intensified sanitation and fire protection
Iberian Peninsula	Decreased production	Intensified protection forest management; intensified sanitation and fire protection
Italy (except mountains)	Decreased production	Intensified protection forest management; intensified sanitation and fire protection
Greece Turkey	Decreased production	Intensified protection forest management; intensified sanitation and fire protection

Source: Nilsson and Pitt, 1991.

zone types and boundaries and, when linked to a climate model, the visual-
ization of the impact of any future climate changes on favorable growing ar-
eas for specific types of vegetation (Leemans, 1990a,b; Leemans and Cramer,
1991).

Climatic records with lengths of between 10 and 40 years during the pe-
riod from 1931 to 1960 were used for calculating mean monthly temperature,
precipitation, and cloudiness data. The final data set contained readings for
some 6,100 land-based weather stations characterized by longitude, latitude,
and altitude. By means of an appropriate interpolation scheme, this array of
selected stations could be used to create a global monthly temperature, pre-
cipitation, and cloudiness database for land areas on a grid with a resolution
of 0.5° (about 55 km at the equator).

The resulting data in each grid point were then used to develop sets of
indicators relevant to the so-called Holdridge life-zone classification system
(*Figure 4*). This scheme relates vegetation zones to climate indicators that
can be derived from basic monthly temperature and precipitation readings.
The three indicators upon which the system relies are biotemperature (based
on the length of and temperature during the growing season), mean annual
precipitation, and a potential evapotranspiration ratio that links biotempera-
ture with annual precipitation and defines different humidity provinces. The
three climatic indicators can be displayed graphically in a logarithmically
scaled triangle, so that each separate life-zone becomes equally significant.

Using combinations of these three indicators derived from the climate
data, a global life-zone map can be developed that, by comparison with
actual vegetation zones, can be used to show the effect of current climate in
determining vegetation patterns (*Figure 5*).

Because these patterns correspond to the present distribution of veg-
etation types, the global life-zone map can also be used for assessing the
effect of a future climate change on vegetation zones. This is done using a
General Circulation Model (GCM) which has been run under current CO_2
conditions and under conditions of a doubling of the atmospheric CO_2 con-
centrations. From this model the differences in mean monthly temperature,
precipitation, and cloudiness are derived. After interpolation between the
GCM grid and the grid of the GVM's climate database, these differences are
then added to the respective values of the present climate database. Again,
a Holdridge life-zone classification can be derived and from that a global
life-zone map which reflects changed climatic conditions. For convenience,
the differences to the global life-zone map which reflects current climatic
conditions are shown in *Figure 6*. The differences show the zones where a
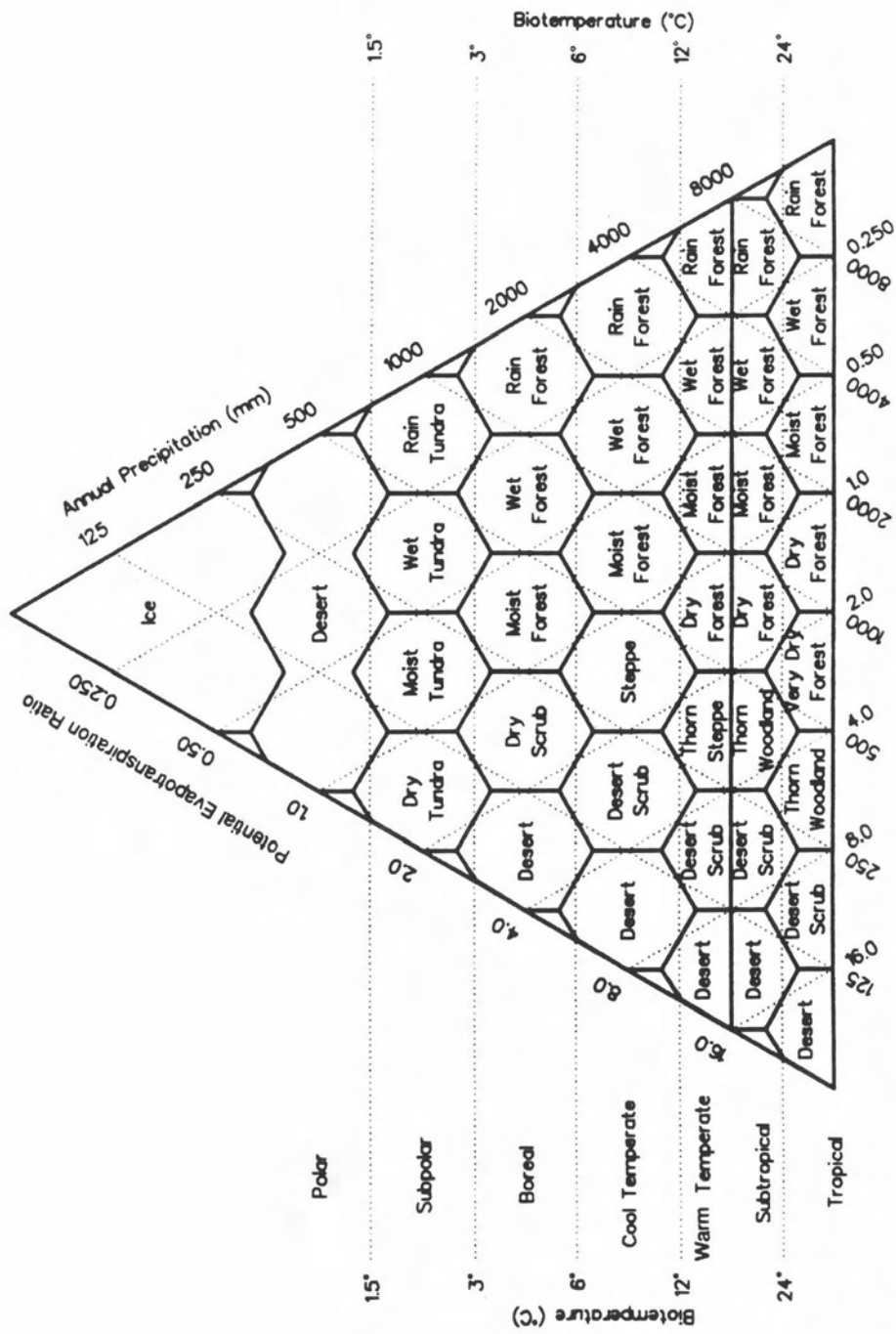
Figure 4. Holdridge world life-zone classification. Source: Leemans, 1990b.
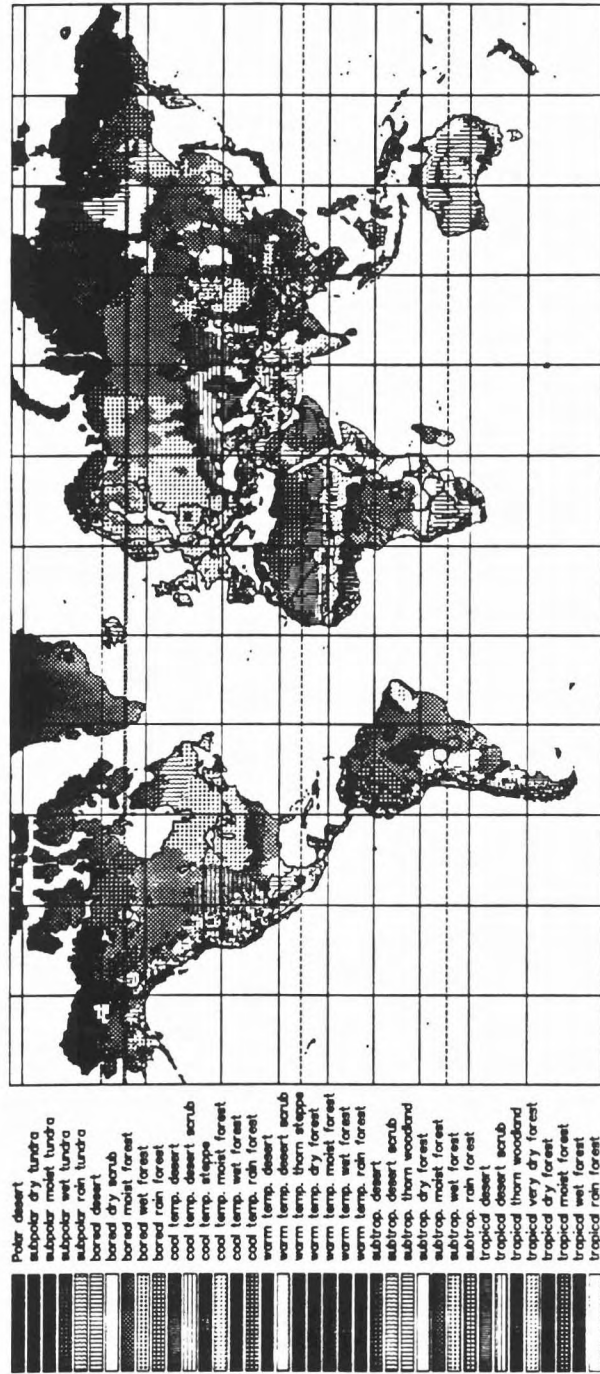
10

Figure 5. A world map from the Holdridge life-zone classification based on a 0.5° gridded temperature and precipitation database. Source: Leemans, 1990a.

change in vegetation is expected to occur; this is in about 60% of the global land area (Leemans, 1990a).

Again, as in the case of TAM, we have to be very careful with final conclusions. Even if we remedy the static behavior of the GVM by linking it to an integrated climate model and letting it respond to transitional CO_2 changes, the model still lacks crucial information on important components such as the nutrient and carbon cycle, soil moisture, and the physiological effects of climate change (Nilsson and Pitt, 1991).

2.3 Regional Acidification INformation and Simulation (RAINS) model

The third environmental impact model available at IIASA is the *Regional Acidification INformation and Simulation (RAINS) model* of the Transboundary Air Pollution Project.

The RAINS model (Alcamo *et al.*, 1990) deals primarily with the acidification of Europe's environment and with sulfur and nitrogen depositions (SO_2, SO_4, NO_x, NH_3) that lead to acidification. The model also examines related problems such as the direct impact of airborne SO_2 on forests. RAINS organizes information and computations about sulfur and nitrogen into three categories: pollution generation and control (including costs), atmospheric transport and deposition, and environmental impacts (*Figure 7*). Each category is represented in RAINS by one or more submodels. Since the principal aim is to provide a temporal-spatial overview of acidification in Europe, the time and space scales of RAINS are accordingly large. The model covers all of Europe, including the European part of the former Soviet Union, with a resolution 150-by-150-km (EMEP[1]grid) for emissions and atmospheric processes, and 0.5° latitude by 1.0° longitude for environmental impacts (*Figure 8*).

Simulations extend back to 1960 for a historical perspective and forward to 2040 to ensure that the long-term consequences of different control policies are taken into account. Because of the large spatial coverage and time horizon, the time step of calculations is also rather large (one year or more).

The *atmospheric processes* portion of the RAINS model calculates the atmospheric transport of emitted sulfur and nitrogen and where these emissions are deposited throughout Europe. For calculating the depositions,

---

[1]Co-operative Programme for Monitoring and Evaluation of the Long-Range Transmission of Air Pollutants in Europe.
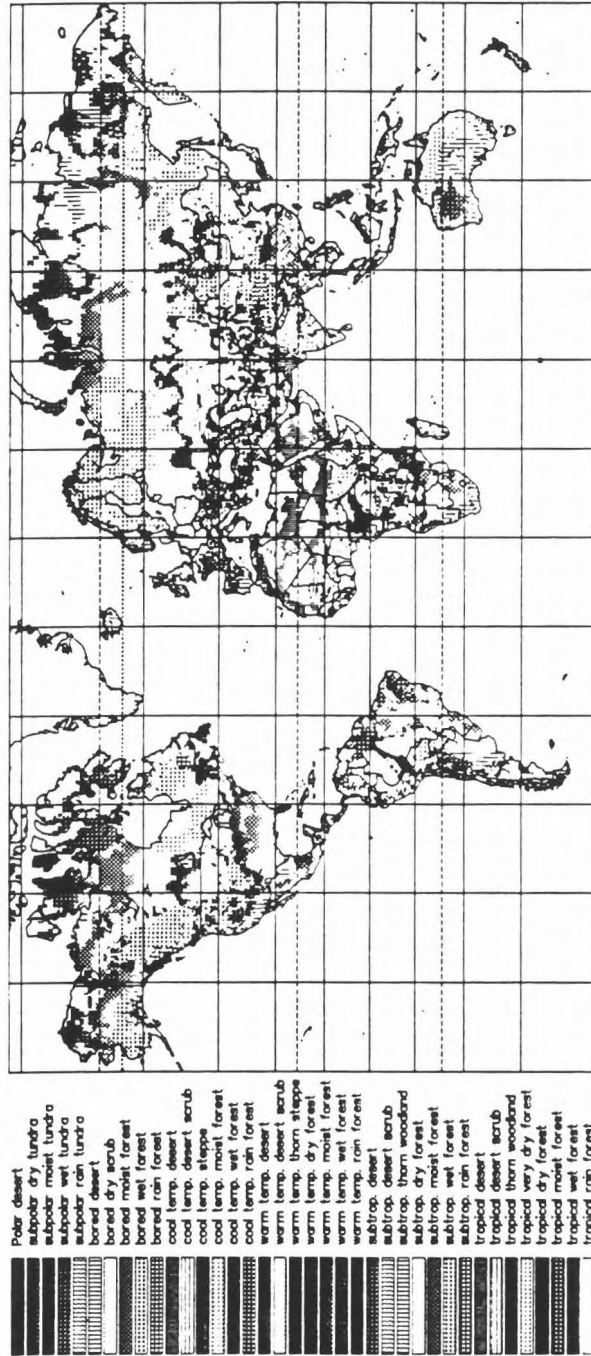
12

Figure 6. A Holdridge life-zone world map with the differences between present climate and a double CO_2 future climate. The marked areas are the original life zones, determined on the basis of present climate. Source: Leemans, 1990a.
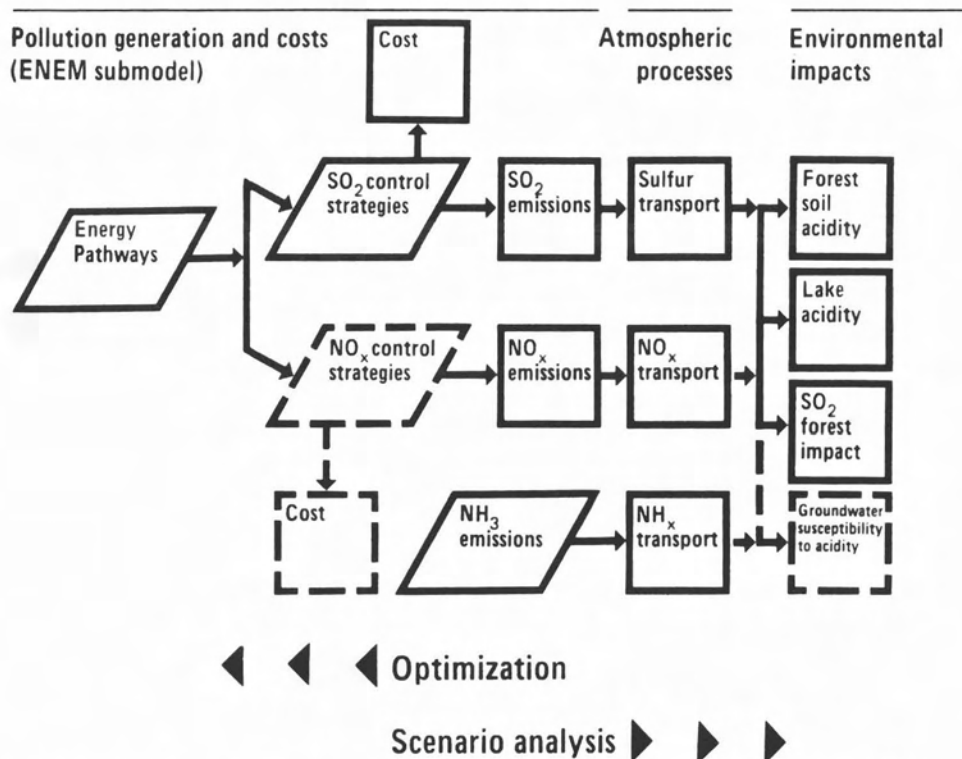
Figure 7. Flowchart of the RAINS model. Source: Alcamo *et al.*, 1990.

RAINS makes use of a linear relationship, so-called *source-receptor (SR) matrices* that express the relationship between country emissions and deposition in each grid point. The SR matrices are computed by the EMEP *Long-Range Transport (LRT) models* of sulfur and nitrogen for Europe. These models, in turn, incorporate the effects of wind, mixing height, precipitation, and other meteorological and chemical variables on sulfur and nitrogen air concentrations and depositions.

Current reduction plans and emission estimates of sulfur and nitrogen compounds indicate that the acid rain phenomenon, although most likely reduced in magnitude, will remain an ecological concern in Europe in the coming decades. Moreover, acidification may mobilize heavy metals accumulated over time in soils which, in turn, may disturb soil organisms, the decomposition of organic matter, and thus the entire nutrient cycle. Therefore, there seems to be a special need for assessing the environment under changed
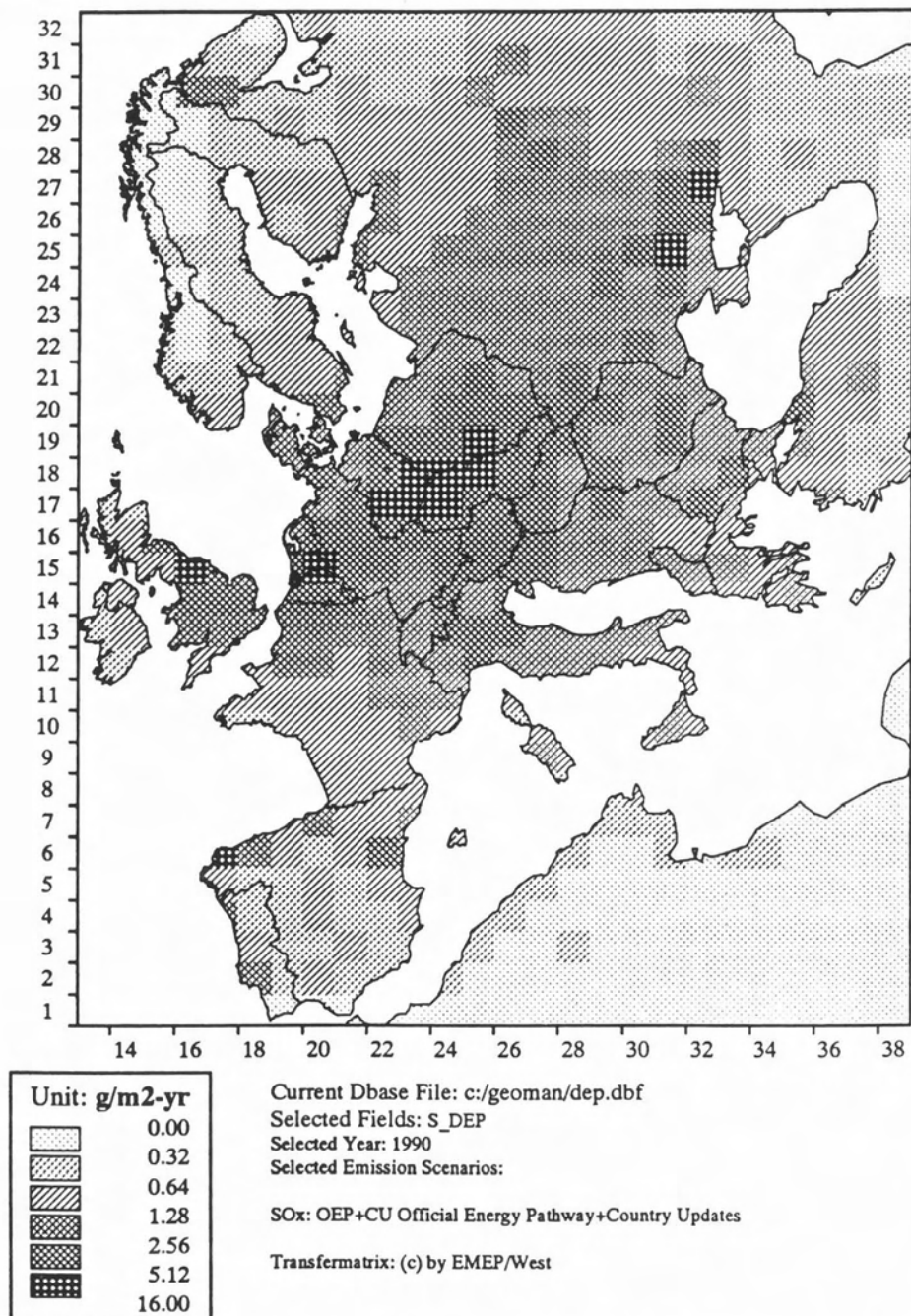
Figure 8. Sulfur deposition for the year 1990, no abatement. Source: RAINS 6.0.

climatic conditions, especially with respect to precipitation and the long-range transport of sulfur and nitrogen and their depositions in combination with that of selected heavy metals (As, Cd, Pb, Zn). Ultimately, this means that new SR matrices have to be derived which reflect changed transport patterns (*Figure 9*).

At present we are considering how to provide the required meteorological input data without necessarily having to use a GCM as a climate model. We would rather use a simpler model, say an EBM, the output of which would be mainly temperature and precipitation. One approach could be to parameterize some of the remaining meteorological quantities in terms of a single variable, say temperature, a procedure which is frequently applied by EBM modelers.

3. The Integrated Model to Assess the Greenhouse Effect

The phrase "integrated climate model" needs to be specified in more detail, especially with respect to the *Intergovernmental Panel on Climate Change (IPCC)*. The IPCC is placing increasing emphasis on the use of time-dependent impact models that are linked with energy-emission accounting frameworks and models that predict in a time-dependent fashion important variables such as atmospheric concentrations of greenhouse gases, temperature, and precipitation. Integrating these tools (greenhouse gas emission strategies, atmospheric processes, ecological impacts) into what is called an integrated assessment model will assist policy makers in the IPCC and elsewhere in assessing the impacts of a wide variety of emission strategies. To be useful to decision makers, an integrated assessment model must have a reasonably quick turnaround time and must give results which are in good agreement with GCMs (*Figure 10*). GCMs, although they are extremely useful as tools for scientific research, are too time-consuming and thus too costly to be used for policy analyses. This means that the integrated assessment model should not compete with GCMs but be complementary to them and take advantage of the scientific results from them.

The *Integrated Model to Assess the Greenhouse Effect (IMAGE)* represents such an integrated assessment model which already combines most of these needs (*Figure 11*). This policy-oriented simulation model has been developed by the Netherlands National Institute of Public Health and Environmental Protection (RIVM) for the calculation of historical and future

16

POLICY OPTIONS
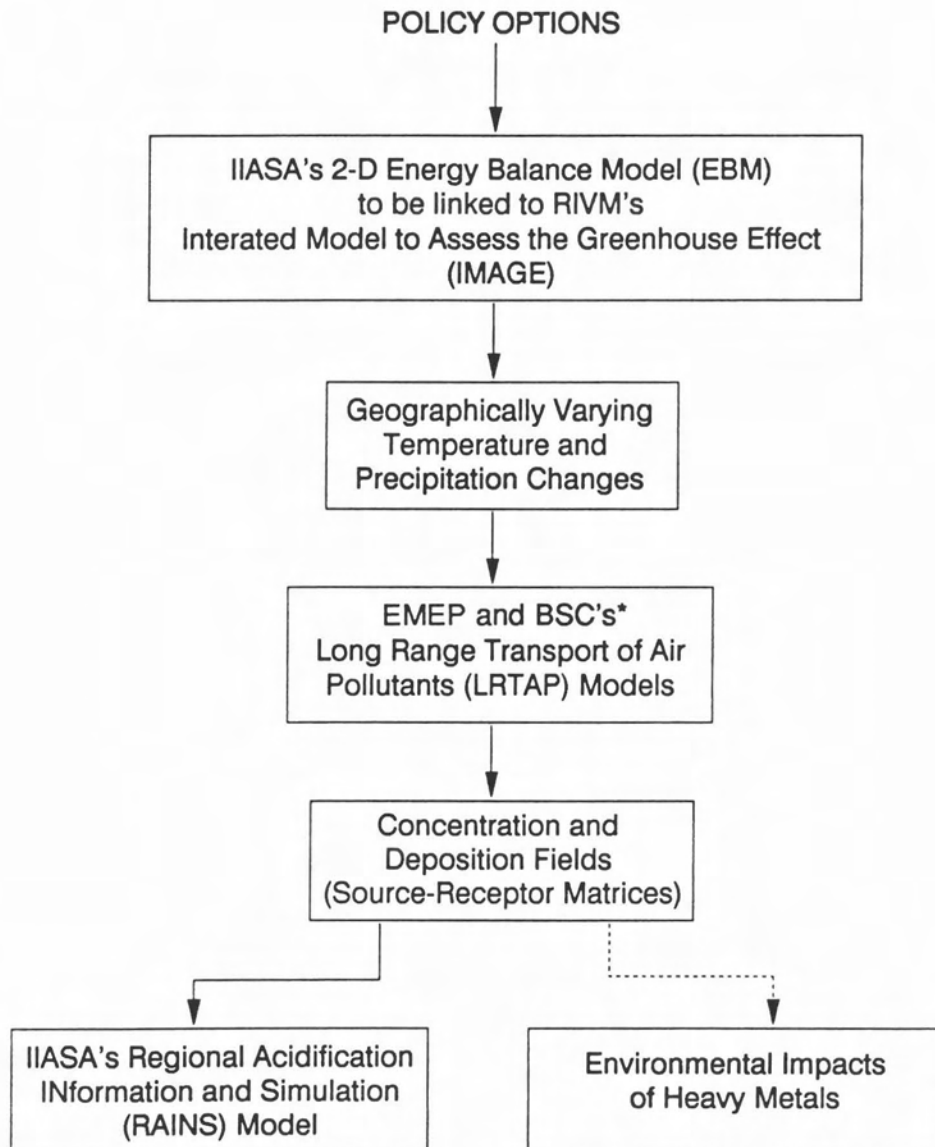
*IBM Bergen Environmental Sciences and Solutions Centre (BSC).

Figure 9. Linkages between models to assess environmental impacts of air pollutants and heavy metals under changed climate.
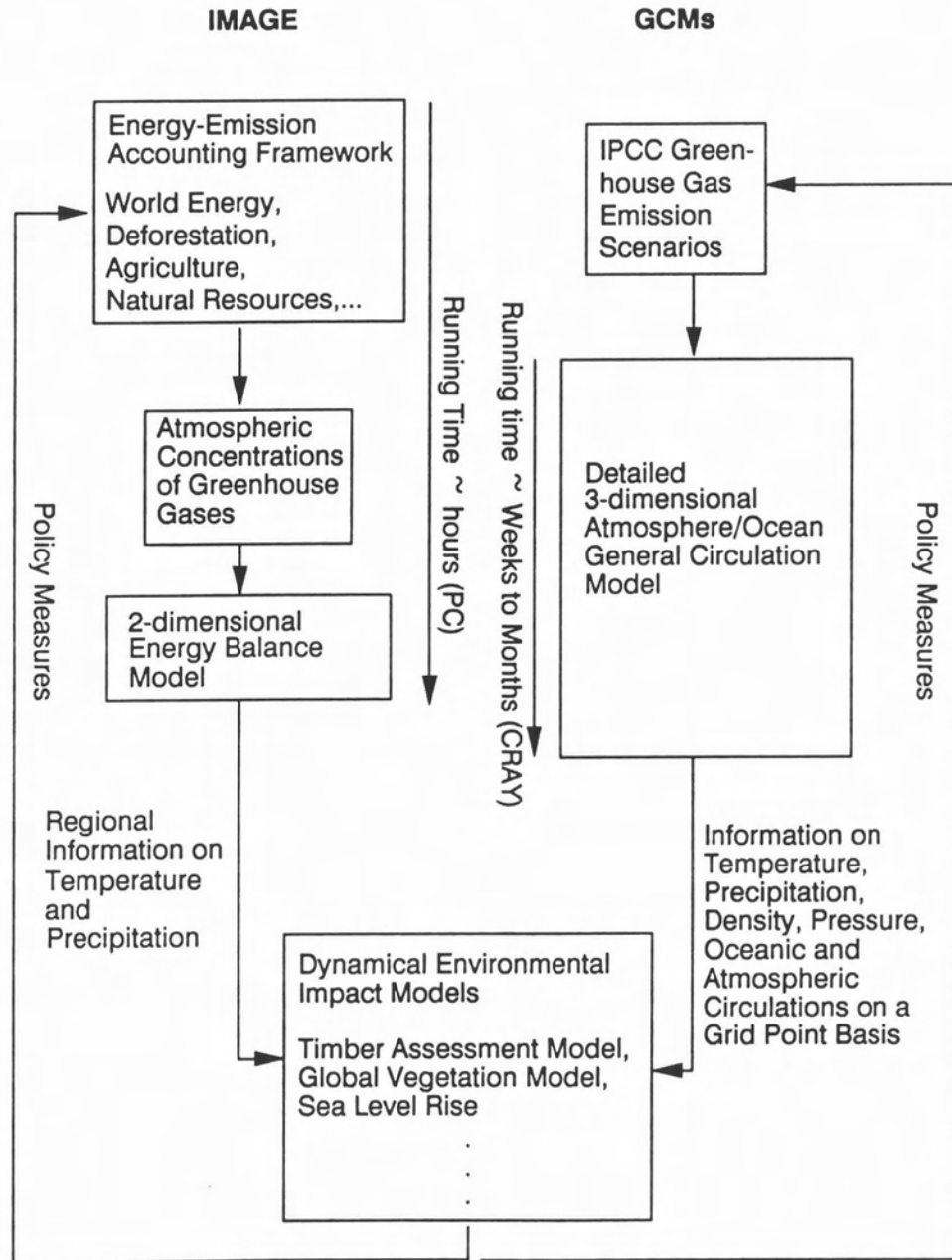
IMAGE

GCMs

Energy-Emission
Accounting Framework

World Energy,
Deforestation,
Agriculture,
Natural Resources,...

IPCC Green-
house Gas
Emission
Scenarios

Running Time ~ hours (PC)

Running time ~ Weeks to Months (CRAY)

Atmospheric
Concentrations
of Greenhouse
Gases

Detailed
3-dimensional
Atmosphere/Ocean
General Circulation
Model

Policy Measures

Policy Measures

2-dimensional
Energy Balance
Model

Regional
Information on
Temperature
and
Precipitation

Information on
Temperature,
Precipitation,
Density, Pressure,
Oceanic and
Atmospheric
Circulations on a
Grid Point Basis

Dynamical Environmental
Impact Models

Timber Assessment Model,
Global Vegetation Model,
Sea Level Rise

.
.
.

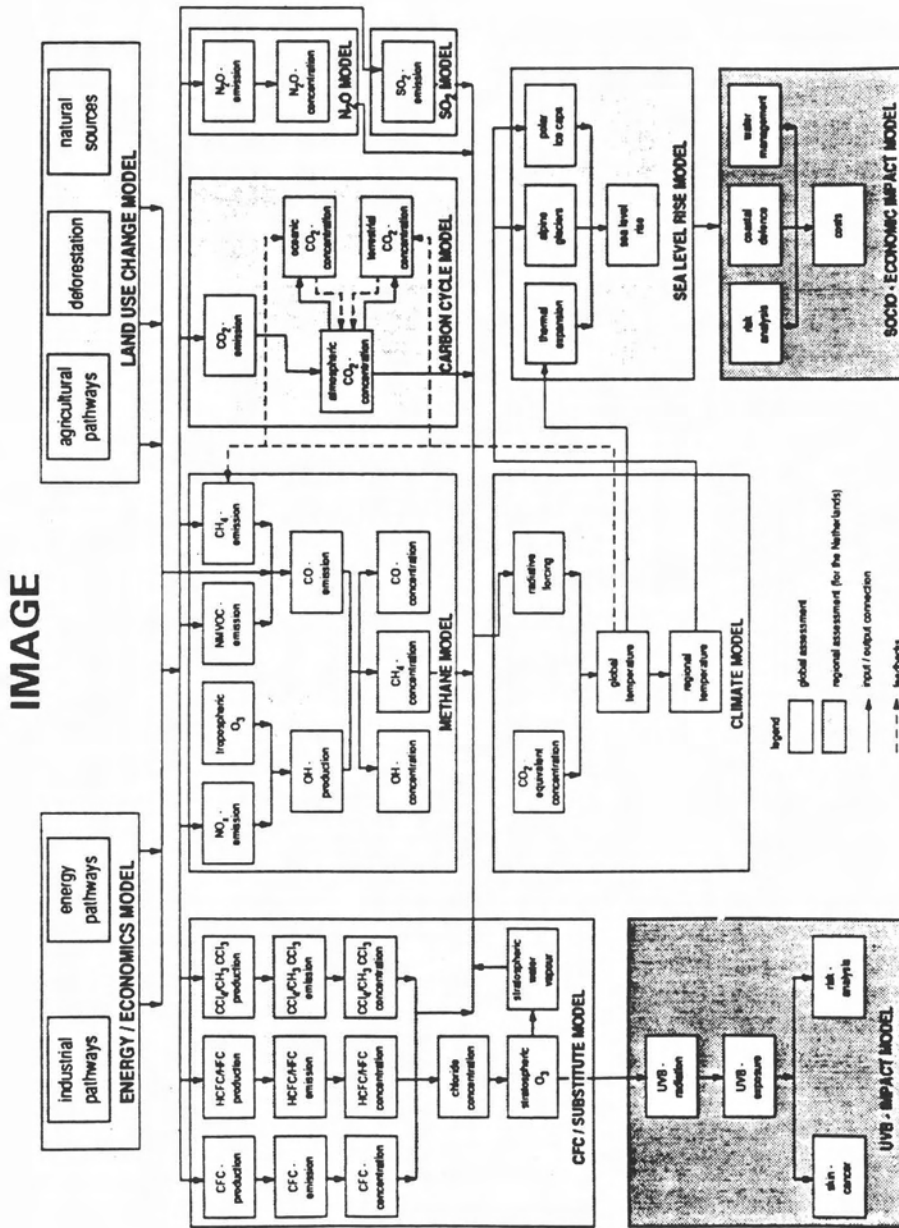**Figure 10.** Integrated model structures.

18

Figure 11. Flowchart of IMAGE. Source: den Elzen *et al.*, 1991.

effects of greenhouse gas emissions on global surface temperature, sea-level rise, and other ecological and socioeconomic impacts (Rotmans, 1990).

3.1 Present climate module of IMAGE

To link it with the environmental impact models, IMAGE needs to have its output modified to produce geographically varying key quantities, say temperature and precipitation, rather than the currently available global mean values. In collaboration with RIVM, this is being done within IIASA's Climate Change Projections Study by incorporating a 2-D EBM into IMAGE.

However, for educational purposes, there is some merit in understanding how the present global climate model within IMAGE works. It is based on Wigley and Schlesinger's (1985) EBM and consists of two atmospheric boxes, one over land with zero heat capacity and the other over an oceanic mixed layer coupled to a diffusive deeper ocean with 50 layers. On time scales relevant to CO_2 forcing, the atmosphere may be assumed to be in equilibrium with the underlying surface. If we simplify the deep ocean to consist of only one layer instead of 50, we are even able to describe the behavior of the system analytically [see *Figure 12*, equations (1) to (5)]. The model is described by equations (3) to (5) where ΔT_L, ΔT_{aL}, ΔT_{a0}, and $\Delta T(t)$ are temperature changes for the land, atmosphere over land, atmosphere over ocean, and oceanic mixed layer, respectively, induced by a radiative forcing $\Delta Q(t)$ at the tropopause; f is the fraction of the globe covered by land; λ is the climate feedback parameter; and k and k_{as} are coefficients used for describing land-ocean and air-sea heat transfer processes, which are assumed to be linear to a first approximation. The variable R_m is the bulk heat capacity (also called thermal inertia) of the mixed layer and ΔF is the change in heat flux at the bottom of the mixed layer.

The basic equations behind equations (3) to (5) are equation (1) and its time-dependent generalization, equation (2). Equation (1) summarizes our current understanding of the steady-state or (instantaneous) equilibrium temperature change ΔT_i due to a radiative forcing ΔQ in an extremely simple global climate model. The climate feedback parameter λ includes all feedbacks that act to displace temperature from or restore it to its equilibrium value in the absence of ΔQ. As we can see, equations (3) and (4) are derived from equation (2) by area-weighting a completely land- and ocean-covered earth and by taking into account heat exchange processes between the different thermal reservoirs, as it is also done for the mixed layer [equation (5)].
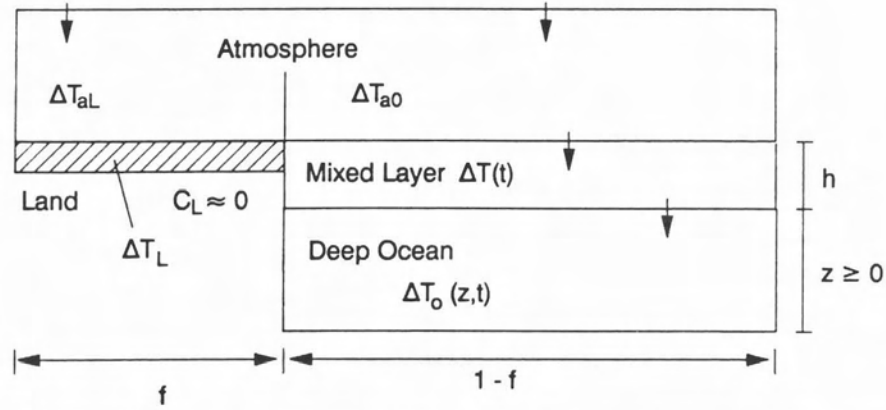
$$\lambda \Delta T_i = \Delta Q \tag{1}$$

$$R\frac{d\Delta T}{dt} + \lambda \Delta T = \Delta Q \tag{2}$$

ΔT_i	global equilibrium temperature change
$\Delta T(t)$	global temperature change
$\Delta Q(t)$	radiative forcing at tropopause
λ	global climate feedback parameter
R	global thermal inertia

$$f\lambda \Delta T_{aL} + k(\Delta T_{aL} - \Delta T_{a0}) = f\Delta Q \tag{3}$$

$$(1-f)\lambda \Delta T_{a0} + k(\Delta T_{a0} - \Delta T_{aL}) + (1-f)k_{as}(\Delta T_{a0} - \Delta T) =$$

$$= (1-f)\Delta Q \tag{4}$$

$$R_m\frac{d\Delta T}{dt} + k_{as}(\Delta T - \Delta T_{a0}) + \Delta F = 0 \tag{5}$$

$\Delta T_L = \Delta T_{aL}$	temperature changes for land resp. atmosphere over land,
ΔT_{a0}	atmosphere over ocean, and
$\Delta T(t)$	mixed layer
f	land fraction
k, k_{as}	land-ocean resp. air-sea heat exchange coefficient
R_m	thermal inertia of mixed layer
ΔF	change in heat flux at bottom of mixed layer

Figure 12. Source: Wigley and Schlesinger, 1985.

We still need to specify ΔF, the change in heat flux at the bottom of the mixed layer – that is, at $z = 0$ [equation (6); see *Figure 13* for equations (6) to (11)]. Here ρ is the density, c the specific heat capacity, and κ the thermal diffusivity of the deep ocean whose temperature change due to ΔQ is $\Delta T_o(z, t)$. The depth below the mixed layer is given by $z \geq 0$ and $\Delta T_o(z, t)$ by equation (7). After inserting the equations into each other, the entire system can be approximated by a first-order ordinary differential equation [equation (8)], say for ΔT, the temperature change in the mixed layer.

Let us now jump forward to the solution where we assume that equation (8) is exponentially forced according to equation (9). Usually, IMAGE calculates annual ΔQ values from the accumulated greenhouse gas concentrations in the atmosphere, based upon empirical relationships. Here we only want to make use of the relationship for CO_2 which illustrates the well-known fact that the radiative forcing is proportional to the logarithm of the concentration ratio [equation (10)] where $C = C(t)$ is the concentration at time t; C_o is the initial ($t = 0$) or preindustrial concentration, say in 1850; and ΔT_{2x} is the change in global equilibrium temperature due to a doubling of CO_2 concentration or simply climate sensitivity (see, for example, Augustsson and Ramanathan, 1977). An exponential form of ΔQ then corresponds to CO_2 variations given by equation (11). It is only important to keep in mind that observed CO_2 changes can be fitted to this form.

There are two ways of presenting the solution, say for 1980, of the following uncertain parameters: C_o, the preindustrial CO_2 concentration in 1850; h, the mixed layer depth; κ, the thermal diffusivity of the deep ocean; and ΔT_{2x}, the global climate sensitivity. Let us first examine *Figure 14* where only h is held constant at 70 m. We are interested in $\Delta T / \Delta T_i$, the ratio of mixed layer temperature change to global equilibrium temperature change. The departure of this ratio from unity is a measure of the degree of disequilibrium due to oceanic thermal inertia effects. The most important result is the wide range of uncertainty in the disequilibrium ratio, say from 0.42 to 0.79 in the case of $C_o = 270$ ppmv. We find that $\Delta T / \Delta T_i$ decreases as ΔT_{2x} increases (that is, the higher the climate sensitivity the more the system is out of equilibrium for a given forcing by 1980) and as κ increases (that is, the higher the thermal diffusivity, the more heat is taken up by the deep ocean). The disequilibrium ratio can also be translated into a time lag L by which the warming in the mixed layer in 1980 lags behind the global equilibrium temperature change.

For the same example (that is, for $C_o = 270$ ppmv), this time lag varies from 14 to 48 years. If the climate sensitivity is as high as some model results

22

$$\Delta F = -\rho c \kappa \left(\frac{\partial \Delta T_o}{\partial z} \right)_{z=o} \tag{6}$$

$\Delta T_o(z,t)$	temperature change of deep ocean
ρ	density
c	specific heat capacity
κ	thermal diffusivity

$$\frac{\partial \Delta T_o}{\partial t} = \kappa \frac{\partial^2 \Delta T_o}{\partial z^2} \tag{7}$$

Combing all equations and solving for $\Delta T(t)$ yields a first order type of ordinary differential equation

$$\frac{d\Delta T}{dt} + \{ \ldots \} \Delta T = \{ \ldots \} \Delta Q \tag{8}$$

$\{\ldots\}$	tunable constants

$$\Delta Q = bt \exp(\alpha t) \tag{9}$$

$$\Delta T_i = \frac{\Delta Q}{\lambda} \approx \Delta T_{2x} \frac{\ln(C/C_o)}{\ln 2} \tag{10}$$

ΔT_{2x}	climate sensitivity
$C(t)$	CO_2 concentration
C_o	CO_2 pre-industrial concentration in 1850

$$C = C_o \exp(Bte^{at}) \tag{11}$$

Solution can be expressed analytically in form of disequilibrium ratio

$$\frac{\Delta T}{\Delta T_i} = \ldots$$

Figure 13. Source: Wigley and Schlesinger, 1985.

$$\frac{\Delta T}{\Delta T_i} \text{ for 1980}$$

Disequilibrium ratios and lags (yr)

		C_0								
		250			270			290		
$\Delta T_{2\kappa}$	κ	1	2	3	1	2	3	1	2	3
1.5	$\Delta T/\Delta T_i$	0.81(0.79)	0.76(0.73)	0.72(0.69)	0.79(0.79)	0.73(0.73)	0.69(0.69)	0.74(0.77)	0.68(0.72)	0.63(0.68)
	$\Delta T/\Delta T_{lin}$	0.97(0.96)	0.97(0.95)	0.96(0.94)	0.94(0.95)	0.93(0.94)	0.92(0.94)	0.88(0.93)	0.87(0.92)	0.85(0.92)
	L	18(19)	23(25)	27(29)	14(14)	19(19)	22(22)	11(10)	14(12)	16(14)
	L_{lin}	22(23)	28(29)	33(34)	22(23)	28(29)	33(34)	22(23)	28(29)	33(34)
3.0	$\Delta T/\Delta T_i$	0.68(0.65)	0.60(0.58)	0.56(0.53)	0.64(0.64)	0.57(0.57)	0.52(0.53)	0.58(0.63)	0.51(0.56)	0.46(0.51)
	$\Delta T/\Delta T_{lin}$	0.96(0.93)	0.95(0.92)	0.95(0.91)	0.91(0.92)	0.90(0.91)	0.89(0.90)	0.82(0.89)	0.80(0.88)	0.79(0.88)
	L	31(34)	39(42)	45(47)	26(25)	32(32)	37(36)	19(17)	24(21)	27(24)
	L_{lin}	38(39)	48(48)	54(54)	38(39)	48(48)	54(54)	38(39)	48(48)	54(54)
4.5	$\Delta T/\Delta T_i$	0.58(0.56)	0.50(0.48)	0.45(0.43)	0.54(0.55)	0.47(0.47)	0.42(0.43)	0.48(0.53)	0.41(0.46)	0.36(0.41)
	$\Delta T/\Delta T_{lin}$	0.95(0.91)	0.94(0.90)	0.94(0.89)	0.89(0.90)	0.88(0.89)	0.87(0.88)	0.79(0.86)	0.77(0.86)	0.76(0.85)
	L	42(45)	52(54)	57(60)	35(34)	43(42)	48(47)	26(23)	32(28)	35(31)
	L_{lin}	51(51)	61(61)	67(67)	51(51)	61(61)	67(67)	51(51)	61(61)	67(67)

Values represent variations in the disequilibrium ratio ($\Delta T/\Delta T_i$) and the lag (L) in 1980 for $\gamma = 0.71$ and various values of the diffusivity ($\kappa = 1\text{-}3 \text{ cm}^2 \text{ s}^{-1}$, see refs 4, 9, 22, 23), the CO_2-doubling temperature change ($\Delta T_{2\kappa} = 1.5\text{-}4.5$ K, see ref. 1) and the initial (1850) CO_2 level ($C_0 = 250\text{-}290$ p.p.m.v., a range which spans the most likely range of 260-280 p.p.m.v. given in ref. 14). ΔT and L correspond to CO_2 variations given by equation (15) fitted through 315 p.p.m.v. in 1958 and 338 p.p.m.v. in 1980[15], while ΔT_{lin} and L_{lin} correspond to CO_2 variations given by equation (15) with $\alpha = 0$ fitted through 338 p.p.m.v. in 1980 (that is, to linear radiative forcing). ΔT and L are relatively insensitive to variations in h; $h = 70$m has been used here (ref. 3). The values shown are based on a full numerical solution of equations (3), (6) and (7); while the bracketed figures are those based on the approximate analytical solution (equation (16)) with $\mu = 2.2$ in the linear case and $\mu = 2.7$ otherwise. In the nonlinear case the optimum value of μ depends on C_0, but we have used the value appropriate to $C_0 = 270$ p.p.m.v. throughout.

h = 70 m

Figure 14. Disequilibrium ratios ($\Delta T/\Delta T_i$) and time lags (L) for 1980. Source: Wigley and Schlesinger, 1985.

suggest, then $\Delta T/\Delta T_i \approx 0.5$ and a substantial future warming will occur even in the absence of any further CO_2 increase; policy makers are usually not aware of this point.

The second way of illustrating the overall uncertainty is given in *Figure 15* which shows $\Delta T(1980)$ as a function of initial CO_2 level and CO_2-doubling temperature change. The ΔT values in this figure are compatible with the observed global mean warming of about 0.5°C over the past 100 years, especially when one considers the uncertainties in the observational record. For $260 \leq C_o \leq 280$ ppmv and $1.5 \leq \Delta T_{2x} \leq 4.5$°C, ΔT ranges between 0.26 and 0.96°C for two extreme combinations of diffusivity and mixed layer depth.

In this approach we have considered only CO_2 in defining the radiative forcing $\Delta Q(t)$. However, we could easily repeat the same exercise with CO_2-eq (CO_2-equivalent concentration) instead of CO_2 and thus account for the other greenhouse gases as well. The other gases may have added to the forcing, contributing perhaps as much as 0.2°C to the overall warming since 1960 (Wigley, 1985).

Figure 16 indicates the potential of IMAGE to capture the first-order temperature behavior of a GCM. The globally averaged surface temperature of IMAGE as a function of CO_2-eq is compared with the respective temperature response of the globally and annually averaged GCM of the Max-Planck-Institute in Hamburg (Cubasch *et al.*, 1991), which is forced according to their Scenario A. It resembles Scenario A of the IPCC which reflects the Business-as-Usual Scenario. In this scenario the energy supply is coal-intensive and, on the demand side, only modest efficiency increases are achieved. Carbon monoxide controls are modest, deforestation continues until the tropical forests are depleted, and agricultural emissions of methane and nitrous oxide are uncontrolled. For CFCs, the restrictions of the Montreal Protocol are implemented, albeit with only partial participation.

Using the same climate sensitivity as that of the GCM, the same scenario was also used to run IMAGE. The agreement between the models can be further improved by using the thermal diffusivity of the deep ocean and the mixed layer depth as tuning parameters (Fleischmann *et al.*, 1992).

3.2 Refining the climate module of IMAGE

What steps should be taken to replace the relatively simple climate model within IMAGE by a 2-D EBM? The following activities are now under way:
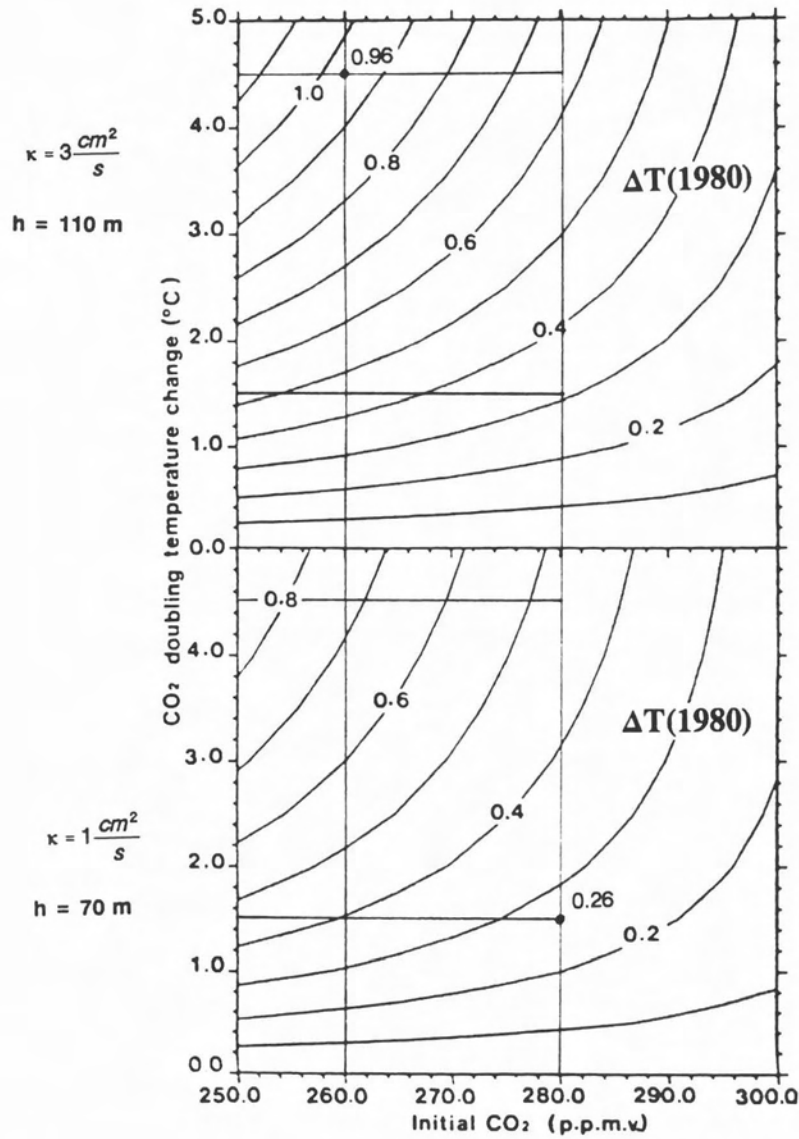
Figure 15. Isolines of temperature change to 1980 (CO_2 level of 338 ppmv) as a function of the CO_2-doubling temperature change and the 1850 initial CO_2 level for two extreme pairs of diffusivity and mixed layer depth. Bottom diagram, $\kappa = 1$ cm^2 s^{-1}, $h = 70$ m; top diagram, $\kappa = 3$ cm^2 s^{-1}, $h = 110$ m. Results are based on our full numerical solution of equations (5), (6), and (7). Source: Wigley and Schlesinger, 1985.
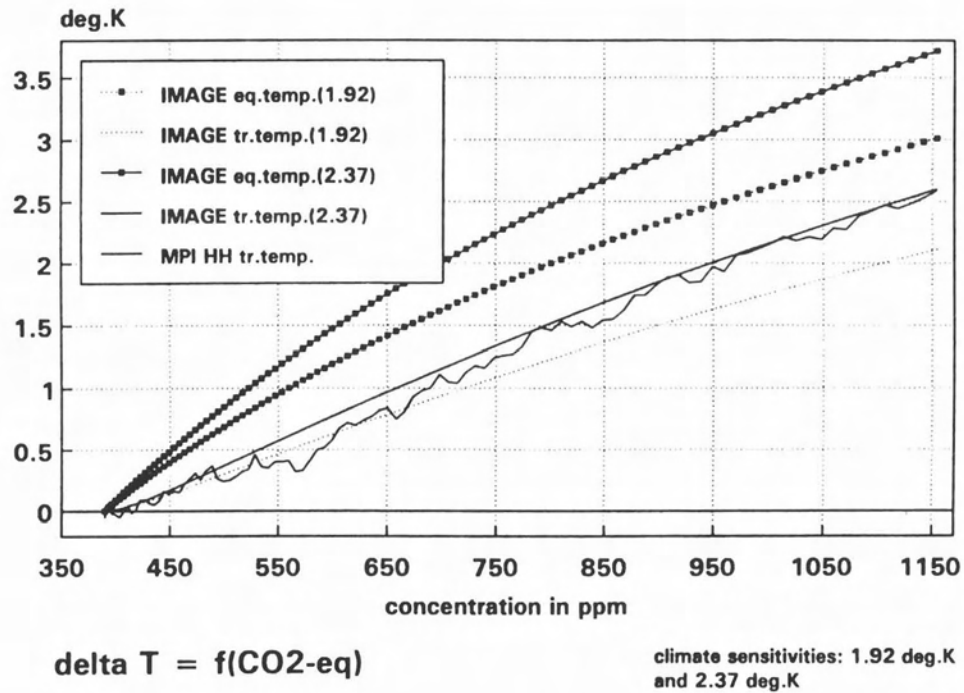
deg.K

- IMAGE eq.temp.(1.92)
- IMAGE tr.temp.(1.92)
- IMAGE eq.temp.(2.37)
- IMAGE tr.temp.(2.37)
- MPI HH tr.temp.

concentration in ppm

delta T = f(CO2-eq)

climate sensitivities: 1.92 deg.K
and 2.37 deg.K

Figure 16. Temperature responses of IMAGE and MPI's GCM. Source: Fleischmann *et al.*, 1992.

- Building a 1-D EBM which gives latitudinally averaged surface temperatures.
- Making use of an existing global *Radiative Convective Model (RCM)* which gives temperature as a function of height, modifying it according to specific needs.
- Building a 2-D EBM by incorporating the RCM; the output will be latitudinally averaged surface temperature and precipitation.

One-dimensional Energy Balance Model (1-D EBM)

We have set up a latitude-dependent EBM of the Budyko-Sellers type (Jonas *et al.*, 1991); it assumes that all energy fluxes into, out of, and between 10° latitude belts can be parameterized by the temperature at the earth's surface. The individual fluxes are schematically represented for the j-th latitude belt
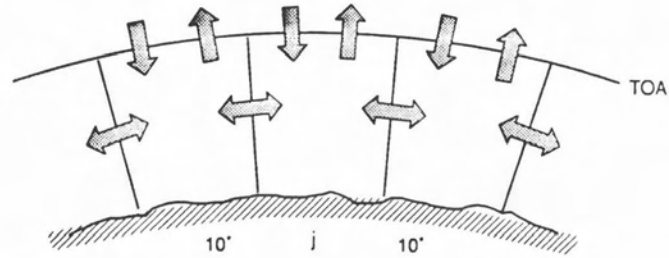
$$\text{(heat stored)}_j = \text{(solar in)}_j - \text{(infrared out)}_j - \text{(net horizontal transport)}_j \qquad (12)$$

$$R_j \frac{dT_j(t)}{dt} = S_j(1 - \alpha_j(t)) - (A(t) + BT_j(t)) - \gamma(T_j(t) - T(t)) \qquad (13)$$

$$\Delta T_j(t) = T_j(t) - T_j(0) \qquad (14)$$

$$R \frac{d\Delta T(t)}{dt} = -S\Delta\alpha(t) - (\Delta A(t) + B\Delta T(t)) \qquad (15)$$

$$R \frac{d\Delta T(t)}{dt} = -\lambda\Delta T(t) + \Delta Q(t) \qquad (2)$$

$$\Delta Q(t) = -\Delta A(t) \qquad (16)$$

$$\lambda\Delta T(t) = S\Delta\alpha(t) + B\Delta T(t) \qquad (17)$$

Figure 17. Source: Jonas *et al.*, 1991.

by equation (12) or in a parameterized form by equation (13) [see *Figure 17* for equations (12) to (17)]. Here the change in latitudinal heat storage of the atmosphere plus the mixed layer is given by the term on the left side of equation (13). Originally, our main interest was in linking the EBM with the radiative forcing as accounted for and handed over by IMAGE; we were not concerned with making it more sophisticated by incorporating a deep ocean. The terms on the right side of equation (13) describe the incoming solar and the outgoing IR flux at the *top of the atmosphere (TOA)*, by which we mean the stratopause here, and the net horizontal energy transport.

We linked the EBM to IMAGE by rewriting equation (13) in terms of a change in zonal surface temperature relative to preindustrial conditions, here taken to be in 1900 [equation (14)], and then globally averaging this equation; we then have equation (15). It relates a change in heat storage with changes in the incoming solar and outgoing IR flux. Here R and ΔT are the globally averaged thermal inertia and surface temperature change; S is the globally averaged solar constant divided by 4 which is assumed constant for our purposes; and $\Delta\alpha$ is the globally averaged albedo change.

The term in parentheses, the change in outgoing IR radiation, requires an explanation. The respective flux [equation (13)] is, strictly speaking, proportional to the fourth power of the characteristic radiating temperature of the earth according to the Stefan-Boltzmann law, but over the small temperature range of interest on the absolute scale this relationship can be considered linear. Following the concept of EBMs, the IR flux at the TOA is even related to surface temperature by $A(t) + BT(t)$, where $A(t)$ and B are empirical parameters designed to account for the greenhouse effect of clouds, water vapor, CO_2, CH_4, N_2O, CFCs, and other greenhouse gases. It is a standard practice to combine the effect of increasing CO_2 or CO_2-eq concentration into the coefficient A. A decrease in $A(t)$ is thought to mimic the radiative effect of an increase in CO_2 but there is no obvious reason why the coefficient B should not change as well. However, for reasons of simplicity let us also adopt this procedure.

Now, by comparing equation (15) with equation (2) in *Figures 17* and *12*, we immediately find that $\Delta Q(t)$ is given by $-\Delta A(t)$ [equation (16)] and $\lambda \Delta T(t)$ by the sum $S\Delta\alpha(t) + B\Delta T(t)$ [equation (17)], where we now omit to specify how to parameterize $\Delta\alpha(t)$ in terms of $\Delta T(t)$. Thus we have identified the linkage by using the radiative forcing calculated by IMAGE.

Figures 18 and *19* show how the EBM behaves when forced by IMAGE according to the IPCC Scenario A. In *Figure 18* the globally averaged temperature response of an EBM, which is subdivided into two hemispheres,
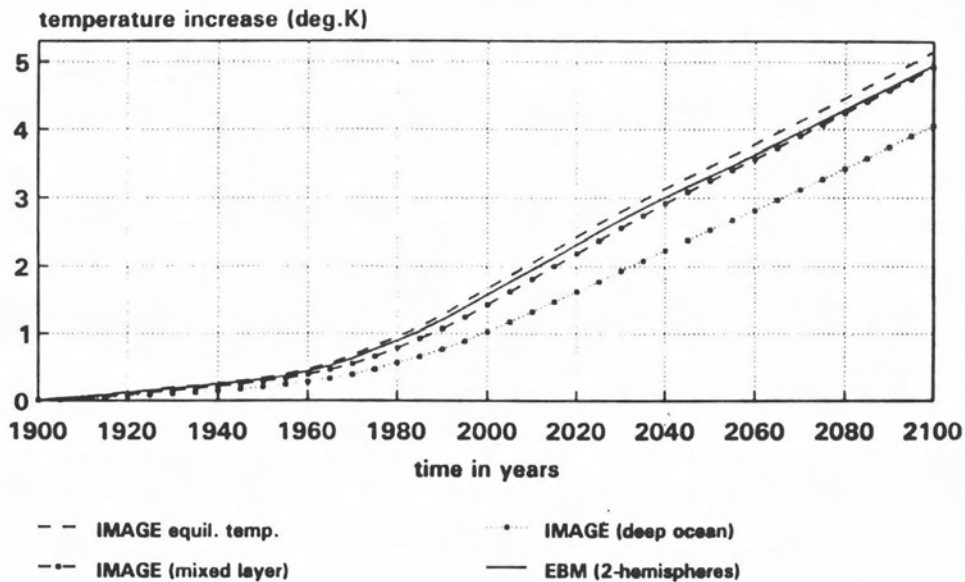
temperature increase (deg.K)

Figure 18. IPCC Scenario A: Basic EBM vs. IMAGE. Source: Jonas *et al.*, 1991, modified.

is compared with the respective run of the original climate model within IMAGE which also incorporates only a mixed layer. Both models agree quite well. In addition, the time-dependent and equilibrium run, two versions of the original climate model, are shown; one accounts for an oceanic heat storage, and the other does not.

In *Figure 19* the latitudinal temperature changes of an EBM consisting of eighteen 10° latitude belts are shown for three time periods. As we can see, the model is strongly influenced by the different parameterizations of the albedo-temperature feedback which we tested. The ice-albedo feedback is somewhat overestimated in the top figure. Because the deep ocean is missing, the latitudinal temperature distributions are rather high. They almost reflect the respective equilibrium distributions if CO_2-eq concentrations would be kept constant from 1990 on, from 2050 on, or from 2100 on, respectively.

Because of its simplicity, the 1-D EBM is well suited for studying the linking procedure to IMAGE. However, two major disadvantages force us to look for a somewhat more sophisticated model:
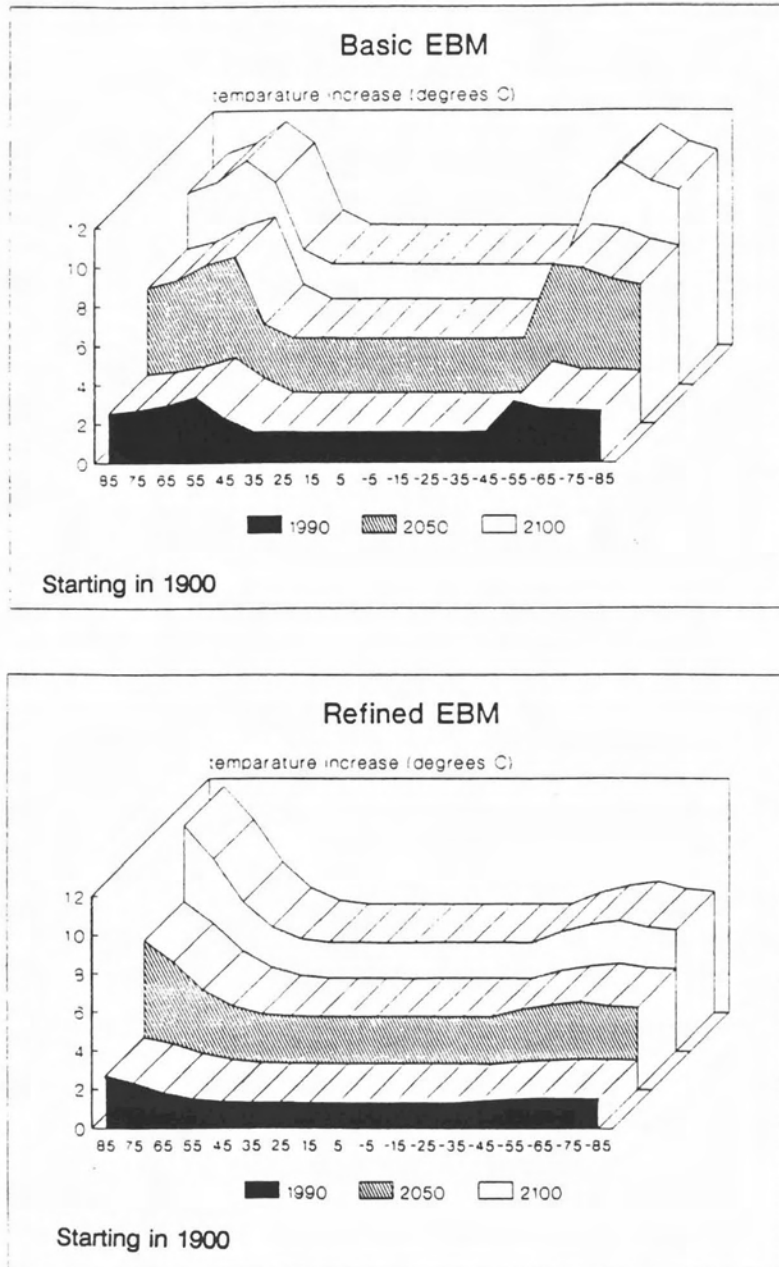
Figure 19. Forced simulation (IPCC Scenario A) with the 18-latitudinal basic and refined EBM. Depicted are the latitudinal temperature responses for three time cuts (1990, 2050, 2100). Source: Jonas *et al.*, 1991.

- A vertically structured atmosphere, which allows one to incorporate precipitation, is missing.

- The linking itself is insufficient. The next climate model should make direct use of the atmospheric CO_2-eq concentration rather than the total radiative forcing derived from it. This is because direct effect $\Delta Q - CO_2$-eq relationships are calculated using detailed radiative transfer models. Such models also incorporate a number of effects, such as the effect of clouds on the transfer of radiation, while the EBM does that as well. Therefore, allowances are made twice for some effects: on the one hand, in radiative transfer models and, on the other hand, in the EBM.

One-dimensional Radiative Convective Model (1-D RCM)

This model was recently developed by MacKay and Khalil (1991) to study the changes in the earth's vertical temperature profile that may be caused by increasing concentrations of CO_2 and other greenhouse gases. *Figure 20* shows the gases considered in the model for the absorption and emission of terrestrial radiation, along with their spectral ranges. With respect to H_2O the absorption of terrestrial radiation is confined to three spectral bands: the vibration-rotational band (centered at 6.3 μm); the pure rotational band (for wavelengths greater than 12 μm); and the continuum band (extending from 8.3 to 20.83 μm).

A total of 14 bands are considered for the 15 μm region for each of the four CO_2 isotopes ($C^{12} O_2^{16}$, $C^{13} O_2^{16}$, $C^{12} O^{16} O^{18}$, $C^{12} O^{16} O^{17}$). A weak absorption band in the atmospheric window region around 10 μm is also included. Broadband IR band absorptances or emissivities are calculated for each model level and with their help the respective IR fluxes, thereby taking into account overlap between the various spectral bands.

As can be seen from *Figure 21*, the solar spectrum extends from about 0.2 to 4 μm with significant absorption due to H_2O, O_3, O_2 and CO_2, under clear sky conditions. The upper solid curve represents the solar spectral irradiance at the TOA and the lower solid curve the solar spectral irradiance at sea level. The area between the upper curve and the shaded region represents the energy reflected by the atmosphere; the shaded region corresponds to the gaseous absorption of the cloudless atmosphere. The principal absorbers in the earth's atmosphere are H_2O in the troposphere and O_3 in the stratosphere. H_2O absorbs primarily in the near-infrared region ($0.7 \leq \lambda \leq 4$ μm) while O_3 is the main gaseous absorber at shorter wavelengths; it is effective in the ultraviolet ($\lambda \leq 0.35$ μm) and the visual ($0.5 \leq \lambda \leq$
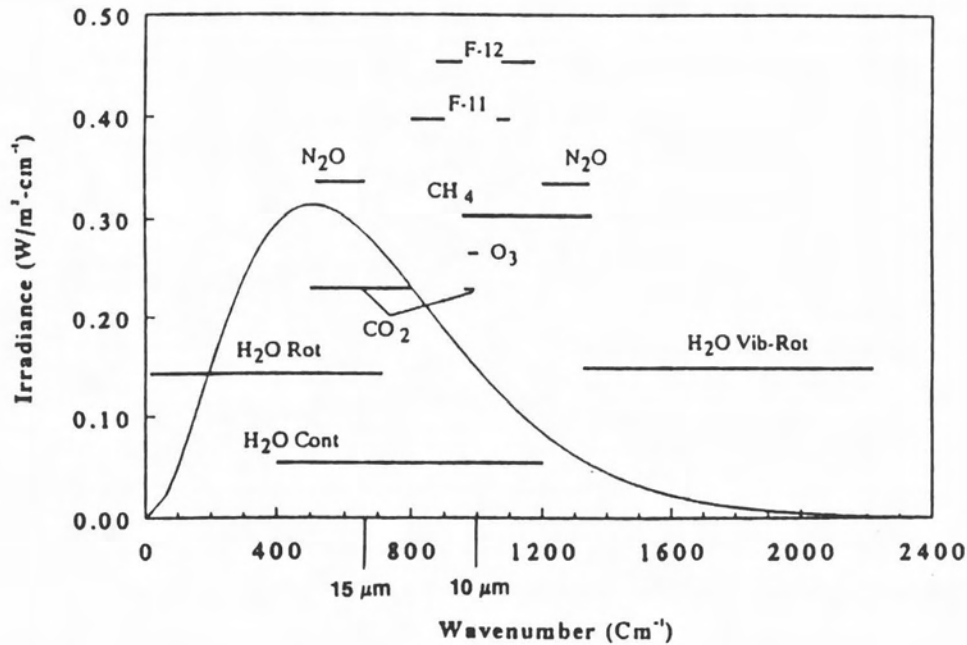
Figure 20. Significant absorbers of terrestrial radiation and their spectral ranges. Also shown is the irradiance for a black body at 260K. Source: MacKay and Khalil, 1991.

0.7 μm) regions. Since Rayleigh scattering is inversely proportional to the fourth power of wavelength, the scattering by air molecules rapidly decreases with increasing wavelength. This explains why Rayleigh scattering is predominant at wavelengths less than 0.8 μm and is negligible beyond.

The method developed by Lacis and Hansen (1974) is used to calculate the solar absorption due to H_2O, O_3 in the ultraviolet region (Hartley and Huggins bands) and the weak absorption by O_3 in the visual region (Chappuis band). CO_2 and O_2 are minor absorbers of solar radiation; together they contribute about 9% to the total atmospheric absorption. The treatment of Sasamori *et al.* (1972) is used to calculate the absorption of solar radiation by CO_2 and O_2.

The model atmosphere contains a single cloud layer covering a horizontal fraction of the sky. The average length of daylight is 12 hours per day, and the average zenith angle 60°. The RCM contains 18 atmospheric layers
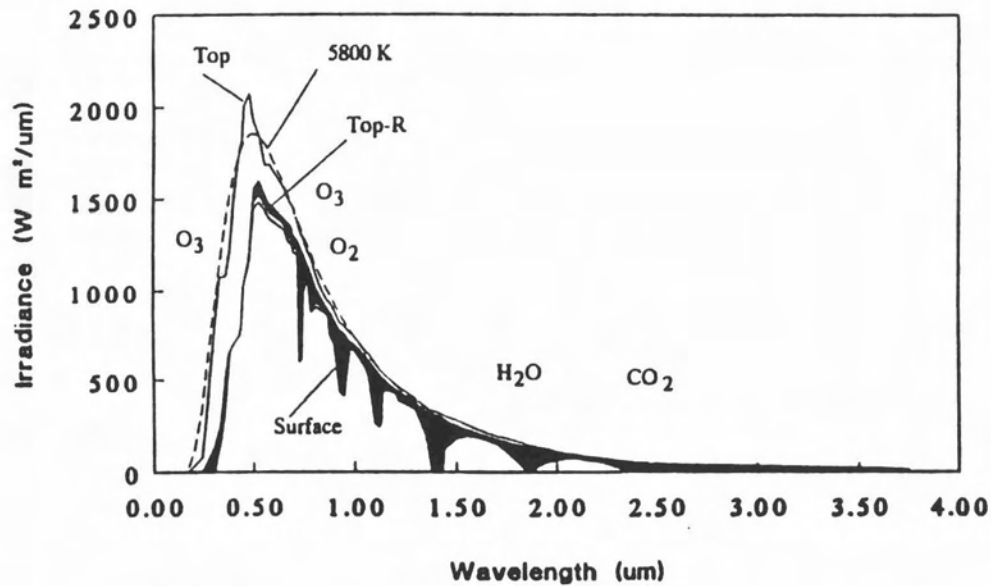
Figure 21. Spectral distribution of solar radiation at the top of the atmosphere (a) and at sea level (b) under clear sky conditions. The shaded region represents the energy absorbed by atmospheric gases and the area between the shaded region and curve (a) represents the energy black scattered by the atmosphere. The dashed curve (c) is the energy curve for a black body at 5800 K. Modified from Liou (1980). Source: MacKay and Khalil, 1991.

with 6 layers above 250 hPa, extending from the surface to an altitude of approximately 40 km (*Figure 22*). For convenience, the σ-coordinate system employed by Manabe and Strickler (1964) is used which allows for layers with a thin pressure thickness near both the earth's surface and the TOA. The inclusion of a nonzero heat capacity for the earth's surface enables the model to estimate the time it takes the earth-atmosphere system to approach equilibrium after some atmospheric perturbation.

The input data are the following: a prescribed profile of relative humidity following Manabe and Wetherald (1967); constant mixing ratios for CO_2, CH_4, N_2O, CFC-11, and CFC-12; and an ozone profile which is based on the 1962 Standard Atmosphere (supplied by the National Climatic Center of NOAA).
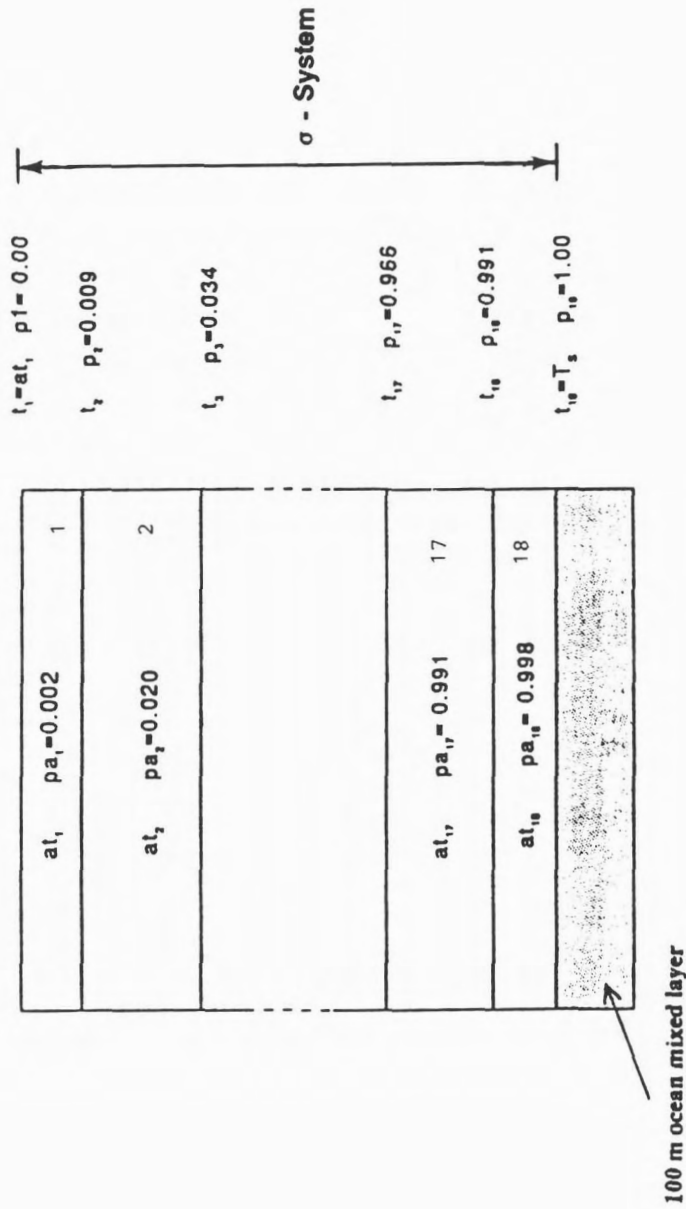
Figure 22. Schematic representation of the 18 layer OGI model of the earth-atmosphere system. The average pressure and temperature of each layer are labeled pai and ati respectively. The pressure and temperature at the top (bottom) of each layer are labeled $p_i(p_{i+1})$ and $t_i(t_{i+1})$. The pressures (in atmospheres) of each layer are assigned as described in the text. Source: MacKay and Khalil, 1991.

Table 2. Results of experiments performed with the OGI 1D RCM to test the sensitivity of the model to various perturbations in input parameters. The standard run was performed with the trace gas concentration profiles; cloud fraction, Ac = 0.5; cloud layer, kap = 11 (4.0 km); surface albedo, rg = 0.10; cloud optical depth, depth = 8.5; solar constant divided by 2, $S_0/2$ = 680 W/m^2; average cosine of zenith angle, μ = 0.50; mean ocean mixed layer depth of 2.5 m; and computational time step of 0.30 days.

Perturbation	ΔT (K)	
Standard	0.0	
1.02 * solar constant	+ 2.2	
Ac = 0.4	+ 3.1	
depth = 8.0	+ 1.8	
kap = 10 (5.1 km)	+ 2.6	
rg = 0.12	− 1.4	
w/o CO_2	−12.8	
w/o CH_4	− 0.7	−14.9 K
w/o N_2O	− 0.6	
w/o Tropospheric O_3	− 0.8	
w/o any O_3	+13.6	

Source: MacKay and Khalil, 1991.

Solar heating and IR cooling rates are calculated for each layer with the help of the respective net fluxes. The equilibrium state of a model atmospheric layer (or the surface) is achieved when the flux of energy (radiant, sensible, or latent heat) into that layer equals the flux of energy out of that layer. Also at equilibrium, the net flux of solar radiation absorbed by all layers and the surface equals the net flux of IR radiation given off at the TOA.

Let us now examine the sensitivity of the model to various perturbations in input parameters. In *Figure 23* the vertical thermal structure predicted for uniform CO_2 concentrations of 320 and 640 ppmv are compared. This CO_2 doubling results in an increase of surface temperature due to an increase of the natural greenhouse effect. The surface temperature change of 1.93K compares favorably with similar studies (e.g., Lindzen *et al.*, 1982; Ramanathan *et al.*, 1987; Hansen *et al.*, 1981). We also recognize a large cooling in the stratosphere due to enhanced radiative cooling to space, an effect which has been noted by many investigators.
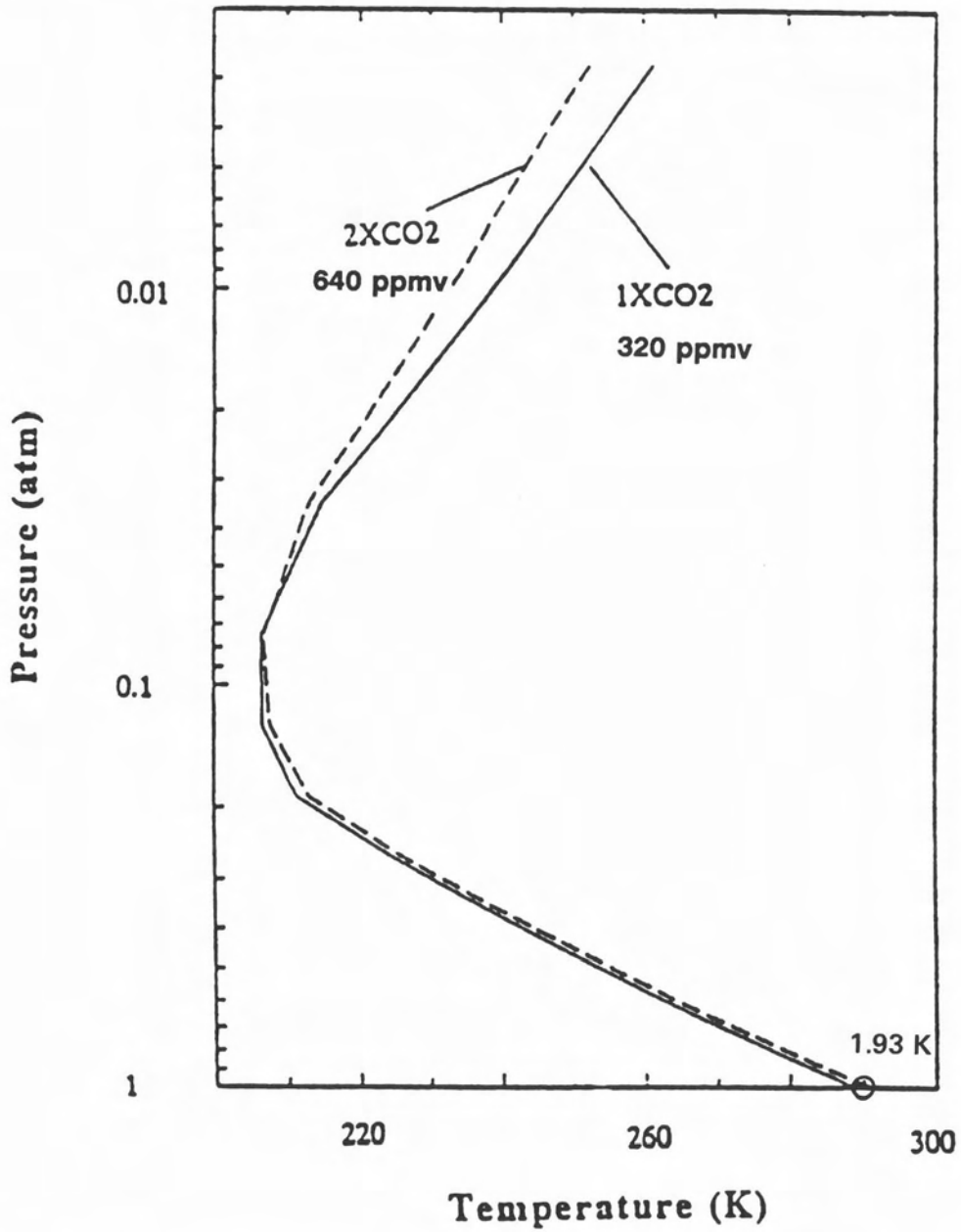
Figure 23. Vertical thermal structure predicted by the OGI model for CO_2 concentrations of 320 ppmv ($1 \times CO_2$) and 640 ppmv ($2 \times CO_2$). Source: MacKay and Khalil, 1991.

Table 2 lists the results of further experiments. We see that the surface temperature changes by 2.2K for a 2% increase in solar constant which is often cited in the literature as being equivalent to a doubling of CO_2. Decreasing the cloud fraction Ac from 0.5 to 0.4 has the obvious effect of decreasing the planetary albedo. This change results in a surface temperature increase of 3.1K. The decrease of cloud optical depth (measure for the amount of water vapor in a vertical column of unit cross section extending between two specific levels) from 8.5 to 8.0 also decreases the planetary albedo, resulting in a 1.8K surface temperature increase, and increasing the surface albedo from 0.10 to 0.12 results in a 1.4K surface temperature decrease. A change in cloud height from 4.0 to 5.1 km results in a surface temperature increase of 2.6K since the lower cloud is warmer and hence emits more radiation upward. Thus when the cloud layer is lifted and cools, the surface temperature must increase to compensate for the decrease in outward IR flux to space associated with a cooler cloud.

The last five experiments listed in *Table 2*, show the effect of completely removing each of the greenhouse gases listed. These results give us an idea of the relative importance of each gas to the natural greenhouse warming of approximately 33K. For CO_2, CH_4, N_2O, and tropospheric O_3 the model gives a combined surface warming of 14.9K, i.e., the rest of the 33K warming, about 55%, is due to water vapor.

The scientific background of this model, especially with regard to the task of eventually incorporating more greenhouse gases to become fully compatible with IMAGE, is now being studied.

Two-dimensional Energy Balance Model (2-D EBM)

We intend to use MacKay and Khalil's (1991) 1-D RCM as the core of the 2-D EBM which is to resolve eighteen latitude belts of 10° width and possibly up to eighteen vertical layers (*Figure 24*). The *Multilayer EBM (MLEBM)* approach taken by Peng *et al.* (1982, 1987) basically serves as our basis for the rest of the model. In the first version, the model describes zonally and annually averaged thermodynamic conditions. A heat balance equation for the atmosphere and the surface is used to determine the temperature in each grid element of the 2-dimensional space (*Figure 25*). Temperature is the only prognostic variable of the model, i.e., all heat transport processes, the release of latent heat due to condensation, or the extent of ice and snow cover are parameterized in terms of a temperature field which depends on latitude and pressure. Relative humidity and cloud cover are prescribed and

are held constant during integration. However, the actual amount of water vapor can vary because of its dependence on temperature.

The surface heat balance equation includes sensible and latent heat fluxes, shortwave and longwave radiation fluxes, and the divergence of oceanic heat transport. For the parameterization of sensible heat a bulk formula is used, while the latent heat flux is expressed empirically by the fractional amount of water available for evaporation and the evaporation from a saturated surface which, in turn, is parameterized further. Diffusion is used to parameterize the net horizontal transport by oceans.

The atmospheric heat balance equation includes shortwave heating rates and longwave cooling rates, heating caused by latent heat release, and horizontal and vertical heat transport. The dynamic redistribution of thermal energy in the atmosphere is a rather complex process. A full consideration of it requires no less than a solution of the full set of equations of fluid motion as in a GCM. In the context of this model, in which velocity is not a variable, dynamic transport is treated in a simplified manner, but still retains its essential effect on the thermal field. The 1-D diffusion approach is used in the first instance, and a 2-D diffusion approach, which is based on a model of baroclinic waves (Stone, 1974), will be considered later.

Finally, the precipitation rate is computed as the residual of the surface evaporation rate and the divergence of water vapor in a vertical column since both must balance in a steady-state atmosphere. Once the precipitation rate is known, it is used in the computation of the heating rate due to atmospheric latent heat release, together with a parameter describing its relative vertical distribution. This parameter, in turn, is based upon the fact that most latent heat release occurs within large-scale stratified clouds in extratropical regions and within convective clouds in the tropics.

This and other parameterizations are currently being implemented and tested against observations, and eventually being replaced by better ones. Besides becoming acquainted with the scientific background of all parameterizations, we are also studying the possibility of reducing the number of vertical layers; so far the radiative computations represent the most expensive part of the 2-D EBM from a computational point of view.

4. Summary

We think that there is an increasing interest in the use of integrated assessment models in the study of global change. Parts of such models may
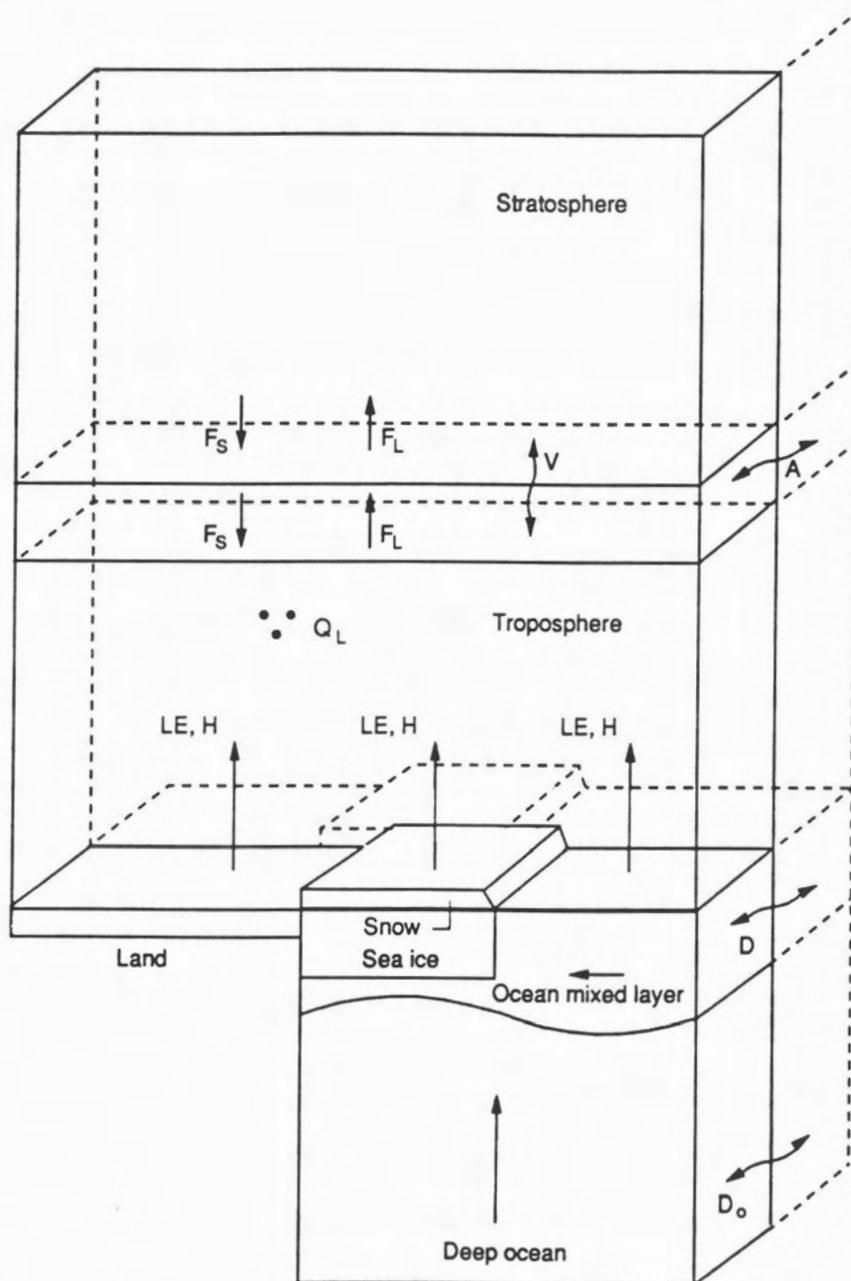
Figure 24. Structure of multilayer EBM. Source: After Peng *et al.*, 1987.

Surface:

$$H + LE + S + I + D = 0 \qquad [\text{Wm}^{-2}]$$

H ... upward sensible heat flux

LE ... upward latent heat flux

S ... upward net flux of solar radiation

I ... upward net flux of infrared radiation

D ... divergence of heat transport by the oceans

Atmosphere:

$$Q_s + Q_I + Q_L + A = 0 \qquad [\text{K day}^{-1}]$$

Q_s ... heating rate due to solar radiation

Q_I ... heating rate due to infrared radiation

Q_L ... heating rate due to latent heat release

A ... heating rate due to dynamical redistribution of heat

Figure 25. Source: Peng *et al.*, 1982.

be simpler versions of more complex models and thus be complementary to them and take advantage of the scientific results from them (e.g., by tuning). An integrated assessment model should concentrate on evaluating environmental effects of first and, if possible, higher orders in an integrated fashion. Also, to be useful to decision makers, an integrated assessment model must have a reasonably quick turnaround time. Results from one or more of the environmental impact models described should be available soon.

References

Alcamo, J., R. Shaw, and L. Hordijk, 1990. *The RAINS Model of Acidification*. Kluwer Academic Publishers, Dordrecht, The Netherlands.

Augustsson, T., and V. Ramanathan, 1977. A Radiative-Convective Model Study of the CO_2 Climate Problem. *J. Atmos. Sci.* **34**:448–451.

Cubasch, U., K. Hasselmann, H. Höck, E. Maier-Reimer, U. Mikolajewicz, B.D. Santer, and R. Sausen, 1991. *Time Dependent Greenhouse Warming Computations with a Coupled Ocean-Atmosphere Model*. Report No. 67. Max-Planck-Institut für Meteorologie, Hamburg, Germany.

den Elzen, M.G.J., J. Rotmans, and M. Vloedbeld, 1991. *Modelling Climate Related Feedback Processes*. Report No. 222901007. RIVM, Bilthoven, The Netherlands.

Döös, B.R., 1991. Environmental Issues Requiring International Action. In *Environment and Development*. MECCA, ÖGUT – Info 14, Vienna, Austria.

Fleischmann, K., U. Nitschke, M. Jonas, K. Olendrzyński, and R. Shaw, 1992. Estimation of GCM Temperature Trend for Different Emission Scenarios with the help of the Integrated Model to Assess the Greenhouse Effect (IMAGE). WP-92-11. IIASA, Laxenburg, Austria.

Hansen, J., D. Johnson, A. Lacis, S. Lebedeff, P. Lee, D. Rind, and G. Russell, 1981. Climate Impact of Increasing Atmospheric Carbon Dioxide. *Science* **213**(4511):957–966.

IPCC, 1990. *Climate Change: The IPCC Scientific Assessment*. Report prepared for the Intergovernmental Panel on Climate Change by Working Group I. J.T. Houghton, G.J. Jenkins, and J.J. Ephraums (eds.). Cambridge University Press, Cambridge, UK.

Jonas, M., M. den Elzen, and K. Olendrzyński, 1991. *A Time Dependent Zonally Averaged Energy Balance Model to be Incorporated into IMAGE (Integrated Model to Assess the Greenhouse Effect)*. CP-91-16. IIASA, Laxenburg, Austria.

Lacis, A.A., and J.E. Hansen, 1974. A Parameterization for the Absorption of Solar Radiation in the Earth's Atmosphere. *J. Atmos. Sci.* **31**:118–133.

Leemans, R., 1990a. *Possible Changes in Natural Vegetation Patterns due to a Global Warming*. WP-90-8. IIASA, Laxenburg, Austria.

Leemans, R., 1990b. Ecological and Agricultural Aspects of Global Change. In *The Environmental Implications of Global Change*. IUCN, Cambridge, UK.

Leemans, R., and W.P. Cramer, 1991. *The IIASA Database for Mean Monthly Values of Temperature, Precipitation, and Cloudiness on a Global Terrestrial Grid*. RR-91-18. IIASA, Laxenburg, Austria.

Lindzen, R.S., A.Y. Hou, and B.F. Farrell, 1982. The Role of Convective Model Choice in Calculating the Climate Impact of Doubling CO_2. *J. Atmos. Sci.* 39:1189–1205.

MacKay, R.M., and M.A.K. Khalil, 1991. Theory and Development of a One Dimensional Time Dependent Radiative Convective Climate Model. *Chemosphere* 22(3–4):383–417.

Manabe, S., and R.F. Strickler, 1964. Thermal Equilibrium of the Atmosphere with a Convective Adjustment. *J. Atmos. Sci.* 21:361–385.

Manabe, S., and R.T. Wetherald, 1967. Thermal Equilibrium of the Atmosphere with a Given Distribution of Relative Humidity. *J. Atmos. Sci.* 24(3):241–259.

Nilsson, S., and D. Pitt, 1991. *Mountain World in Danger*. Earthscan Publications Limited, London, UK.

Nilsson, S., O. Sallnäs, and P. Duinker, 1991. *Forest Potentials and Policy Implications: A Summary of a Study of Eastern and Western European Forests by the International Institute for Applied Systems Analysis*. ER-17. IIASA, Laxenburg, Austria.

Nilsson, S., O. Sallnäs, and P. Duinker, 1992. *Future Forest Resources of Western and Eastern Europe*. The Parthenon Publishing Group, Carnforth, Lancs, UK.

Peng, L., M.-D. Chou, and A. Arking, 1982. Climate Studies with a Multi-Layer Energy Balance Model: I. Model Description and Sensitivity to the Solar Constant. *J. Atmos. Sci.* 39(12):2639–2656.

Peng, L., M.-D. Chou, and A. Arking, 1987. Climate Warming due to Increasing Atmospheric CO_2: Simulations with a Multilayer Coupled Atmosphere-Ocean Seasonal Energy Balance Model. *J. Geophys. Res.* 92(D5):5505–5521.

Ramanathan, V., L. Callis, R. Cess, J. Hansen, I. Isaksen, W. Kuhn, A. Lacis, F. Luther, J. Mahlman, R. Reck, and M. Schlesinger, 1987. Climate-Chemical Interactions and Effects of Changing Atmospheric Trace Gases. *Rev. Geophys.* 25(7):1441–1482.

Rotmans, J., 1990. *IMAGE: An Integrated Model to Assess the Greenhouse Effect*. Kluwer Academic Publishers, Dordrecht, The Netherlands.

Sasamori, T., J. London, and D.V. Hoyt, 1972. Radiation Budget of the Southern Hemisphere. *Meteor. Monogr.* 13(35):9–23.

Stone, P.H., 1974. The Meridional Variation of the Eddy Heat Fluxes by Baroclinic Waves and their Parameterization. *J. Atmos. Sci.* 31:444–456.

Wigley, T.M.L., 1985. Carbon Dioxide, Trace Gases and Global Warming. *Climate Monitor* 13(5):133–148.

Wigley, T.M.L., and M.E. Schlesinger, 1985. Analytical Solution for the Effect of Increasing CO_2 on Global Mean Temperature. *Nature* 315:649–652.